

Development of a Web-Based Control System for a Heliostat Test Facility

by
Hein Joubert

Thesis presented in partial fulfilment of the requirements for the degree of Master of Engineering (Mechanical) in the Faculty of Engineering at Stellenbosch University



Supervisor: Dr Jaap Hoffmann
Co-supervisor: Dr Willie Smit

April 2019

The financial assistance of the National Research Foundation (NRF) towards this research is hereby acknowledged. Opinions expressed and conclusions arrived at, are those of the author and are not necessarily to be attributed to the NRF.

Declaration

By submitting this thesis electronically, I declare that the entirety of the work contained therein is my own, original work, that I am the sole author thereof (save to the extent explicitly otherwise stated), that reproduction and publication thereof by Stellenbosch University will not infringe any third party rights and that I have not previously in its entirety or in part submitted it for obtaining any qualification.

Copyright © 2019 Stellenbosch University

All rights reserved



UNIVERSITEIT • STELLENBOSCH • UNIVERSITY
jou kennisvennoot • your knowledge partner

Plagiaatverklaring / *Plagiarism Declaration*

- 1 Plagiaat is die oorneem en gebruik van die idees, materiaal en ander intellektuele eiendom van ander persone asof dit jou eie werk is.
Plagiarism is the use of ideas, material and other intellectual property of another's work and to present is as my own.
- 2 Ek erken dat die pleeg van plagiaat 'n strafbare oortreding is aangesien dit 'n vorm van diefstal is.
I agree that plagiarism is a punishable offence because it constitutes theft.
- 3 Ek verstaan ook dat direkte vertalings plagiaat is.
I also understand that direct translations are plagiarism.
- 4 Dienooreenkomstig is alle aanhalings en bydraes vanuit enige bron (ingesluit die internet) volledig verwys (erken). Ek erken dat die woordelikse aanhaal van teks sonder aanhalingstekens (selfs al word die bron volledig erken) plagiaat is.
Accordingly all quotations and contributions from any source whatsoever (including the internet) have been cited fully. I understand that the reproduction of text without quotation marks (even when the source is cited) is plagiarism.
- 5 Ek verklaar dat die werk in hierdie skryfstuk vervat, behalwe waar anders aangedui, my eie oorspronklike werk is en dat ek dit nie vantevore in die geheel of gedeeltelik ingehandig het vir bepunting in hierdie module/werkstuk of 'n ander module/werkstuk nie.
I declare that the work contained in this assignment, except otherwise stated, is my original work and that I have not previously (in its entirety or in part) submitted it for grading in this module/assignment or another module/assignment.

	H. Joubert

Abstract

This thesis describes the recommissioning of a small heliostat test facility and the development and implementation of a suitable web-based control system. The facility is operational and available for small scale concentrated solar research with 12 heliostats commissioned, having a total mirror area of 24 square meters. Since the facility is to be used for research purposes, the control system was designed to be flexible with an easy start-up and calibration process. The graphical user interface is user friendly and laid out in a logical manner, making it possible for the system operator to control the heliostats in a safe and efficient manner, without requiring much training. Since the graphical user interface is web-based, it can be opened on any device with an internet connection, allowing the operator to control the facility from a smartphone while being amongst the heliostats, or any other location. This feature makes the system robust in the sense that its operation is not dependent on a specific PC, or installed software on a computer or device. The recommissioned Helio40 facility was extensively used to supply concentrated solar radiation for an experimental receiver research project. These tests signified the first active receiver tests to be conducted using the Helio40 facility on STERG's high temperature laboratory located on the roof of the mechanical engineering building at Stellenbosch University.

Opsomming

Hierdie tesis beskryf die heraanleg van 'n klein heliostaat toets fasiliteit en die ontwikkeling en implementering van 'n geskikte web-gebaseerde kontrole-stelsel. Die fasiliteit is operasioneel en beskikbaar vir kleinskaalse gekonsentreerde sonkrag navorsing met 12 operasionele heliostate, met 'n totale spieëlarea van 24 vierkante meter. Aangesien die fasiliteit vir navorsingsdoeleindes gebruik gaan word, is die beheerstelsel ontwerp om aanpasbaar te wees met 'n maklike aanvangs- en kalibrasieproses. Die grafiese gebruikerskoppelvlak is gebruikersvriendelik en logies uitgelê. Dit stel die stelseloperator instaat om die heliostate op 'n veilige en doeltreffende manier te beheer, sonder dat baie opleiding benodig word. Aangesien die grafiese gebruikerskoppelvlak web-gebaseer is, kan dit op enige toestel met 'n internet konneksie geopen word, sodat die operateur die fasiliteit van 'n slimfoon kan beheer buite die grens van die beheerkamer. Hierdie kenmerk maak die stelsel robuust in die sin dat die werking daarvan nie afhanklik is van 'n spesifieke rekenaar, of geïnstalleerde sagteware op 'n rekenaar of toestel nie. Aan die einde van die projek was die funksionele Helio40-fasiliteit gebruik om gekonsentreerde sonstraling vir 'n eksperimentele ontvanger navorsingsprojek te lewer. Hierdie toetse was die eerste aktiewe ontvanger toetse wat uitgevoer was deur gebruik te maak van die Helio40-fasiliteit, deel van STERG se hoë temperatuur laboratorium, geleë op die dak van die meganiese ingenieurswese gebou by Stellenbosch Universiteit.

Acknowledgements

The author would like to acknowledge the National Research Foundation (NRF) for the partial funding of the research project, and colleagues André de Jong and Elias Basson for their support in helping with tracking tests that were carried out, as well as their support in helping to recommission the facility.

Table of Contents

Declaration	i
Abstract	iii
Opsomming	iv
Acknowledgements	v
Table of Contents	vi
List of Figures	ix
List of Tables	xi
Nomenclature	xii
1 Introduction.....	1
1.1 Solar energy.....	1
1.2 Converting solar energy to electrical energy	1
1.2.1 PV	1
1.2.3 CSP	1
1.2.4 Classification of CSP systems	2
Comparison between central receiver and parabolic trough technologies.....	5
1.3 The heliostat control problem	6
1.4 Helio40 facility.....	7
1.5 Objectives.....	9
1.6 Methodology.....	10
1.7 Scope and limitations	10
2 Literature review	11
2.1 Defining the solar position relative to an observer	11
Solar position algorithms.....	12
2.2 Heliostat optics.....	13
2.3 Heliostat tracking error	14
Categorization of tracking error sources.....	15
2.4 Heliostat control strategies.....	17
2.4.1 Classification of control strategies.....	17
2.4.2 Closed loop control	18

2.4.3	Open loop control.....	22
3	Helio40 facility Inspection	27
3.1	Initial facility inspection	27
3.2	General system considerations.....	28
3.2.1	Tracking update frequency	28
3.2.2	Safety considerations.....	29
4	Maintenance done on facility.....	30
4.1	Overhaul of electrical wiring	30
4.2	Levelling of heliostat pod	32
5	Heliostat controller development and testing	34
5.1	First prototype heliostat controller.....	34
5.1.1	Prototype 1 hardware breakdown	34
5.1.2	Heliostat control program version 1.....	35
Functionality	35
Program Structure	36
5.1.3	Tracking performance.....	38
5.2	Second prototype heliostat controller.....	40
5.2.1	Prototype 2 hardware breakdown	40
5.2.2	Prototype 2 Wi-Fi communication.....	41
5.3	Final heliostat controller design (PCB).....	43
Final heliostat controller hardware	43
6	Helio40 graphical user interface (GUI)	45
6.1	Required functionality.....	45
6.2	Outsourcing of GUI & web hosting	45
6.3	Heliostat controller & GUI communication	46
6.4	Graphical user interface (GUI) final version.....	47
GUI breakdown.....		49
7	Functionality of the recommissioned facility	50
7.1	Powering up the facility	50
7.2	Giving the first commands	51
7.3	Calibration	53
7.3.1	Calibration on target.....	53
7.3.2	Calibration on receiver	55

7.4	Tracking and tracking adjustments	55
7.5	Stow and shutdown	56
7.6	Recovering a “lost” heliostat.....	57
	Override heliostat position	57
8	System operation	59
8.1	Utilization of the recommissioned Helio40 facility	59
8.2	Operational findings.....	59
9	Conclusion	62
9.1	Summary of work	62
9.2	Conclusions	62
9.3	Recommendations for future work	63
	9.3.1 Automated calibration offset	63
	9.3.2 Levelling of roof mounted heliostats.....	63
	9.3.3 Safety recommendations for use of facility.....	63
	References	64
	Appendix A. Photos of calibrated sunspots	66

List of figures

Figure 1: Generally accepted CSP technology types (maroon arrows represent reflected sunlight, blue arrows with dashed line represent rotation axis, orange represents the receiver). (Source: (Gauché, et al., 2017))	2
Figure 2: Typical layout of a parabolic trough plant	3
Figure 3: Photos of the 50MW _e Bokpoort parabolic trough plant with 9.3 hours of thermal energy storage	3
Figure 4: Typical layout of a CRS power plant	4
Figure 5: Crescent dunes 110 MW _e CRS plant with 10 hours of thermal storage. (Source: Solar Reserve, [S.a.]	5
Figure 6: Photo of the heliostat facility, part of the Solar Thermal Energy Research Group (STERG) high temperature laboratory, located on the roof of the mechanical engineering building at Stellenbosch University.	8
Figure 7: Earth surface coordinate system for observer at Q showing the solar azimuth angle A, the solar altitude angle (α) and the solar zenith angle (θ_z) for a central ray along direction vector S. (Source: Stine & Geyer 2001)	11
Figure 8: 3D Model showing the annual sun path of Stellenbosch (Source: Marsh, 2014)	12
Figure 9: Heliostat optics	13
Figure 10: Heliostat tracking error	14
Figure 11: Heliostat control strategies classification	18
Figure 12: Satellite image of the Weizmann institutes heliostat field, as well as a receiver design that uses Kribus's method and accepts concentrated radiation all around its circumference.	19
Figure 13: Local feedback from incident light angle sensor located between target and facet	21
Figure 14: Top view of a CRS plant showing the limitations of sensor placement	22
Figure 15: Heliostat calibration incorporating an error correction target	23
Figure 16: Moontracking method	25
Figure 17: Water damage of a heliostat local controller (left) and the roof mounted power relay board (right) that distributes power to the individual local controllers.	27
Figure 18: Illustration of sunspot movement with a 30 second tracking update interval.	28
Figure 19: Heliostat potential permanent eye damage zone	29
Figure 20: Satellite image of high temperature roof laboratory, showing the neighbouring buildings being within the potential eye damage zone.	30
Figure 21: Relay distribution box (left) and the switchboard (right)	31
Figure 22: Rewiring of the switchboard	31
Figure 23: Helio40 power infrastructure (roof mounted heliostats not included in illustration)	32

Figure 24: Eliminating the pedestal tilt.....	33
Figure 25: First prototype heliostat controller	35
Figure 26: Flow diagram of the first heliostat control program	36
Figure 27: Heliostat tracking loop.....	37
Figure 28: Actuator control loop	38
Figure 29: Tracking response of a 2-hour tracking tests of the prototype controller.	39
Figure 30: Second prototype Wi-Fi enabled heliostat controller	40
Figure 31: Wi-Fi communication architecture	41
Figure 32: Final Helio40 controller	44
Figure 33: Mock-up of GUI.....	46
Figure 34: Communication structure between the heliostat controller, SQL database and the GUI	47
Figure 35: Final version of the Helio40 facility Graphical user interface	48
Figure 36: All heliostats offline, signified by the red circles	50
Figure 37: Control panel on the left showing heliostats connected to the Control panel, and the switch board indicating the heliostats are powered with the LEDs.	51
Figure 38: Heliostat field reaches defocused position	52
Figure 39: Defining the defocused position	53
Figure 40: Calibration popup window	54
Figure 41: Illustration of the calibration procedure from the perspective of the control room	55
Figure 42: Tracking aimpoint adjustment.....	56
Figure 43: Typical Helio40 facility test, status flow diagram	57
Figure 44: Final tests being conducted with 12 tracking heliostats	59
Figure 45: Observed tracking drift error.....	60
Figure 46: Experimental receiver after 35 hours of tracking tests were completed.	61
Figure 47: Network outages prevented heliostats from updating their position, causing the heliostat beams to drift.....	61

List of tables

Table 1: Heliostat design choices that determine theoretical heliostat pointing accuracy	15
Table 2: Heliostat misalignment errors	16
Table 3: Average measured misalignment errors before and after levelling.....	33

Nomenclature

Variables

A	aimpoint coordinate	[~]
A	altitude angle	[rad]
B	heliostat coordinate	[~]
O	origin	[~]
T_{hot}, T_{cold}	temperatures of hot and cold energy reservoirs	[K]
α	altitude angle	[rad]
ϵ	angular error	[rad]
η	efficiency	[~]
θ_i	angle of incidence/reflection	[rad]

Vectors and matrices

H	heliostat normal vector	[rad]
R	reflected vector	[rad]
R_i	intended reflected vector	[rad]
S	central solar ray vector	[rad]

Subscripts

H	heliostat
e	electric
e	east
n	north
z	zenith

Abbreviations

ALC	artificial light calibration
CCD	charge-coupled device
CRS	central receiver system
CSP	concentrated solar power
CSS	cascading style sheets
DNI	direct normal irradiation
GUI	graphical user interface
HTF	heat transfer fluid
HTML	hypertext mark-up language
IDE	integrated development environment

I/O	input/output
LCOE	levelized cost of electricity
LED	light emitting diode
PCB	printed circuit board
PV	photovoltaic
SEDC	solar energy development centre
SQL	structured query language
STERG	solar thermal energy research group
TES	thermal energy storage

1 Introduction

This chapter introduces concepts relevant to solar energy, before focussing on the control of heliostats and the Helio40 facility which is the focus of this thesis.

1.1 Solar energy

The sun, a medium sized star in the middle of our solar system constantly provides earth with energy in the form of solar radiation. The radiation from the sun arriving at the earth's atmosphere is in the form of direct normal irradiation (DNI) which is the energy received per unit area with a surface that is always perpendicular to the irradiation. When the solar radiation passes through the earth's atmosphere, scattering and absorption introduce a diffuse component, reducing the original solar input by roughly 30 % on a clear day, to an average of around 1000 W/m² that arrives at earth's surface (Stine & Geyer 2001). Diffuse radiation permits us to see in the shade, and it is characterized by light coming from all different directions other than directly from the disc of the sun, thus it is not possible to concentrate diffuse radiation. On the other hand (as the name implies) DNI can be concentrated, which makes it the only useful component of solar radiation for applications requiring concentration.

1.2 Converting solar energy to electrical energy

The two methods currently used in industry to convert solar energy to electrical energy is the direct method of using Photovoltaic (PV) panels, and concentrated solar power (CSP).

1.2.1 PV

Photovoltaic power systems are very simple in the sense that they only require the PV panels and DC-AC inverters for powering mains voltage equipment. PV panels utilize both the diffuse and direct components of solar radiation, which has seen their deployment at large latitudes that do not receive much DNI. PV panels are inherently modular, leading to these systems powering small electronic devices isolated from the electric grid, to being deployed in vast quantities for utility-scale power generation. Despite the simplicity and modularity of PV systems, the current electrical energy storage technology is not yet economically viable for utility scale electrical energy storage. Thus, simply put, if the sun is not shining, PV power stations do not dispatch electricity. This means that the deployment of solar PV will not solve the base load problem (a steady uninterrupted supply of electrical energy).

1.2.3 CSP

CSP on the other hand, is an indirect electrical power generation method where the solar energy is first converted into thermal energy, which is then used to power a steam turbine connected to an electric generator. Therefore, the power block of a CSP plant operates on the same principle as the power block of a

conventional coal burning power station. The intermediate thermal energy conversion step opens the possibility to store thermal energy in large insulated tanks, which is relatively easy and cost-efficient (Dinter & Möller, 2016). The stored thermal energy can then be deployed (converted into electrical energy) when the solar resource does not match the demand or simply in times of peak demand when energy prices are generally higher.

As mentioned, only the DNI component of solar radiation can be concentrated, which makes it the only useful component for CSP applications. CSP power stations are thus typically built in regions that receive a high annual average DNI to maximise their efficiency and reduce the levelized cost of electricity (LCOE). These regions are typically found on latitudes around $23^\circ \pm 10^\circ$ north and south of the equator (desert/sub tropic regions).

Even though CSP has more technical challenges compared to other renewables, and generally higher capital costs per installed kilowatt, TES that increases the capacity factors of CSP plants have decreased the LCOE and has guaranteed the technology's survival. In a review of renewables by (IRENA, 2018) it is stated that by 2020, commissioned CSP plants will increasingly be delivering electricity at a cost that is within the lower end of the fossil fuel fired cost range.

1.2.4 Classification of CSP systems

CSP systems are categorized into line- or point-focussing systems which are then further divided into continuously curved and discrete reflector types. These methods of concentration are summarized in Figure 1 below.

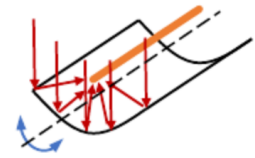
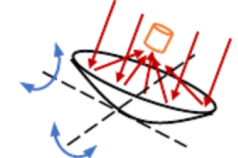
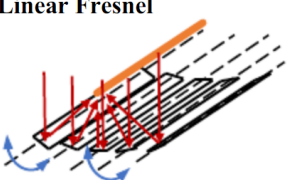
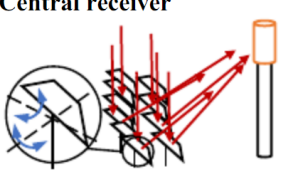
Reflector type	Focus type	
	Line focus (single axis, 2D concentrating)	Point focus (2 axis, 3D concentrating)
Continuous (continuously curved to axes)	Parabolic trough 	Parabolic dish 
Discrete (multiple, near flat)	Linear Fresnel 	Central receiver 

Figure 1: Generally accepted CSP technology types (maroon arrows represent reflected sunlight, blue arrows with dashed line represent rotation axis, orange represents the receiver). (Source: (Gauché, et al., 2017))

The parabolic trough and central receiver collector concepts illustrated in Figure 1 have been the prevailing technologies and will therefore be further discussed specifically focussing on central receiver systems, which is this project's field of research.

Parabolic trough

Parabolic trough plants consist of rows of parabolic trough shaped mirrors that concentrate solar radiation onto receiver tubes (typically a steel tube with an evacuated glass cover for insulation) located along the focal line of the troughs. A thermal oil heat transfer fluid (HTF) is pumped through the receiver tubes and transports the absorbed thermal energy to the power block (the HTF is typically heated to around 393 °C). Here, the HTF both heats up molten salt storage and is pumped through a heat exchanger to generate steam, which in turn drives a steam turbine connected to an electrical generator.

The rows of troughs are aligned north to south and track the sun in one axis from sunrise in the east to sunset in the west. The technology has been in commercial use since the 1980's and is the most implemented CSP technology to date. Figure 2 shows a simplified illustration of the typical layout of a parabolic trough plant.

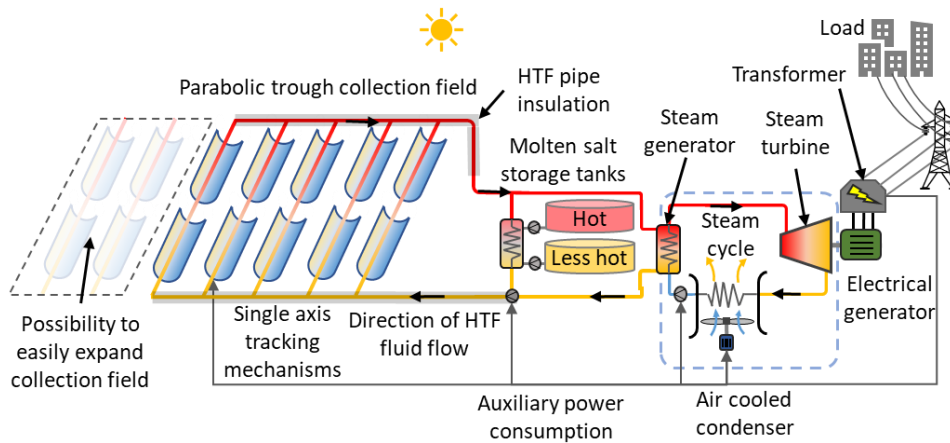


Figure 2: Typical layout of a parabolic trough plant

Figure 3 shows photos of the 50MW_e parabolic trough plant located 18 km north of Groblershoop in the Northern Cape. In the figure, a satellite image is shown with dimensions together with two photos which the author took while visiting the plant in 2017.

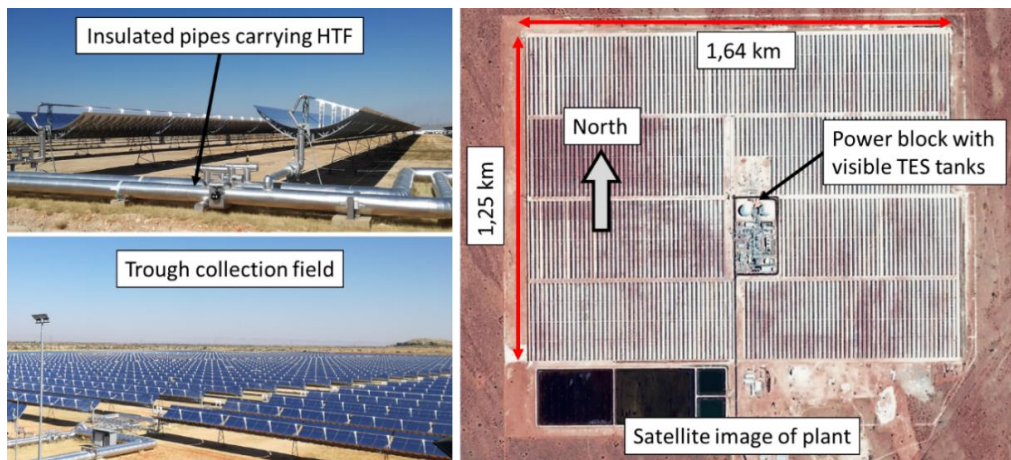


Figure 3: Photos of the 50MW_e Bokpoort parabolic trough plant with 9.3 hours of thermal energy storage

Central receiver

A central receiver solar plant relies on thousands of dual-axis tracking mirrors referred to as heliostats, to reflect the incident solar rays to a thermal receiver at the top of a centrally located tower (Figure 4 shows a simplified illustration of the typical layout of a central receiver plant). The industry trend for central receiver plants has been to use molten salt as the heat transfer fluid and thermal storage, as it eliminates the intermediate heat exchange step between the TES and the receiver. Central receiver plants are also more suited to use molten salt as heat transfer fluid as they operate at higher temperatures, (typically around 566 °C where synthetic oils decompose) and the receiver can be drained of molten salt, eliminating the risk of the salt solidifying in the receiver during the night (the nitrate salts used as HTF solidifies around 220 °C). The power block that converts the thermal energy into electrical energy is identical for both parabolic trough and central receiver power stations, although the condensers are sometimes wet cooled for increased efficiency as will be discussed when comparing the two different plants.

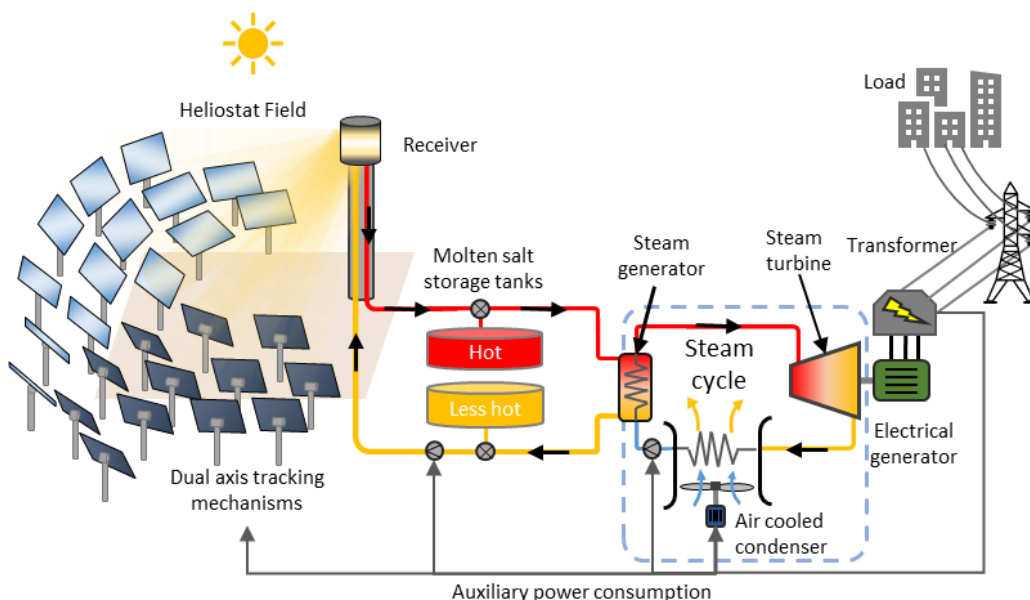


Figure 4: Typical layout of a CRS power plant

Figure 5 shows photos of the Crescent Dunes 110 MWe central receiver plant located 300 km northwest of Las Vegas in Nevada, United States. On the satellite image, the methodical layout of the 10 347 heliostats is visible. The scale of the plant is also indicated, as well as the distance from the furthest heliostat to the base of the tower. Each heliostat has a mirror area of 115.7 m², and the tower is approximately 200 m high (Solar Reserve, [S.a.]).

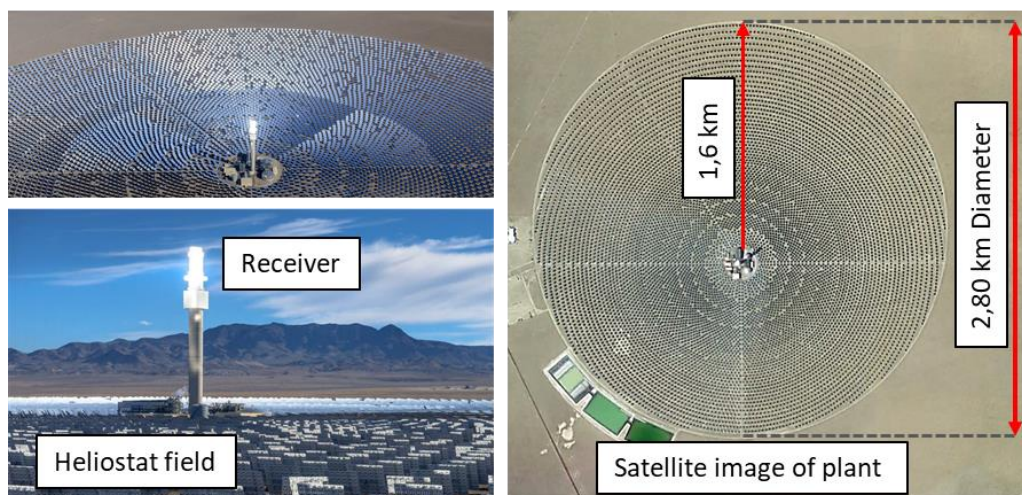


Figure 5: Crescent dunes 110 MWe CRS plant with 10 hours of thermal storage. (Source: Solar Reserve, [S.a.])

Comparison between central receiver and parabolic trough technologies

The single axis tracking parabolic trough collectors have a theoretical solar concentration limit of 212, while point focussing central receiver systems have a theoretical limit of 45000 (Stine & Geyer 2001). These limits are obviously unreachable, and in practice parabolic trough plants reach a concentration ratio of around 80, while CRS achieve around 1000. The higher concentration ratio of point focussing systems relates to a smaller receiver area, which reduces the amount of heat loss, increasing the conversion efficiency of solar energy to usable thermal energy. This is clearly visible when comparing the satellite images of the two plants and realising that parabolic trough plants have kilometres of receiver tubes carrying the HTF where losses are inevitable (approximately 113 km of receiver tubes for the 50 MWe Bokpoort parabolic trough plant).

The upper limit of the theoretical achievable efficiency of a heat engine is expressed by the Carnot efficiency. However, it is well known that the practical heat engines are not as efficient as the classical Carnot cycle. Apart from heat leaks and friction, the fundamental limitation to the efficiency is caused by the rate at which heat can be exchanged between the working material and heat reservoirs, as described by (Curzon & Ahlborn, 1975). The authors show that the efficiency at maximum power output is given by the expression:

$$\eta = 1 - \sqrt{\frac{T_{cold}}{T_{hot}}} \quad (1.1)$$

Inspection of the equation reveals that the greater the difference between the hot and cold temperatures (turbine inlet and heat rejection temperatures for the Rankine cycle), the greater the efficiency. The T_{cold} temperature can be lowered by implementing more effective cooling, however, it is limited by the high daytime temperatures and scarce water sources of the desert climates where solar thermal power stations are usually built. To further improve the efficiency, the T_{hot} temperature must be increased, which can only increase with increasing

concentration ratio. Due to this fact, central receiver systems have the potential to be more efficient than parabolic trough plants. Furthermore, the energy density of the heat transfer fluid increases with temperature, this reduces the required size of the energy storage tanks, decreasing the initial cost of the power station.

A key advantage of parabolic trough plants however, is that the technology is very modular. By adding more loops of troughs to the collection field, the energy collection capacity of the plant can be expanded, illustrated on Figure 2. This property has also eased the design process for different size plants. Central receiver power stations on the other hand are not modular as the tower & receiver and the reflective field are separate components that are specifically sized for each other.

The central receiver power plants are limited by size, due to practical factors and economics. A practical consideration is the required accuracy of the heliostat to reflect the solar radiation onto the receiver, that can be more than a kilometre and a half away as illustrated on Figure 5. As a general rule, the cost of a heliostat increases with an increase in rigidity and attainable positional accuracy. Moreover, the further away the heliostat is from the tower, the smaller its energy contribution due to atmospheric attenuation losses. Thus, beyond a certain distance the energy contribution of a heliostat will no longer justify its initial capital cost, which sets the size limit of the CRS plant.

Despite the theoretical advantages of central receiver systems, the fact that the number of operational trough plants vastly outnumber central receiver plants, is a clear indication that the potential gain in efficiency has not yet overcome the added complexity and cost.

1.3 The heliostat control problem

Most people have at some occasion held a piece of reflective material on a sunny day and reflected the sunlight at another individual or object. It probably went without notice that they solved the heliostat control problem, using the closed loop control method. The eyes (sensors) look at where the reflected beam hits the surroundings (output) and then moving the mirror accordingly (control input), until the reflected beam hits the desired target (eliminating the error).

This (closed loop control) is the most accurate way a heliostat can be positioned/controlled as the output is directly measured, eliminating all the internal and external error sources that may be present. However, if for example 100 colleagues all try to focus their reflected beam on the same target, the ability to distinguish between the individual reflected beams becomes very difficult. The same problem is present if the feedback control method is implemented in a central receiver plant, however a few methods attempting to close the control loop is discussed in the literature review.

The alternative is to go back in the control path and retrieve feedback from the position of the mirror and keep it in the correct orientation as to reflect the sunlight onto the receiver, without checking that the solar beam is actually hitting the receiver (without checking the output). This approach is called the open loop control method. For humans this approach is not possible (trying to reflect the sun onto a target blindfolded by only knowing the required angles the mirror should be positioned in), however, modern heliostats with computer-controlled actuators can make precise position adjustments using their internal rotary/linear encoders.

Open loop control systems work well for tasks that are repetitive, predictable and free from external disturbances, as they have no way of compensating for these error sources. Thus, in theory, the heliostat control problem is perfectly suited for open loop control, as the position of the heliostat relative to the receiver, the kinematic model of the heliostat, and the solar positions can all be very accurately measured or predicted. However, in practice there are various error sources that arise along different stages of the heliostat's commissioning that introduce fixed and time varying tracking errors. These error causing factors are further discussed in section 2.3.

The open loop control method does however require a calibration step before the open loop tracking can start. Calibration of a heliostat is a procedure where the control loop is temporarily closed (measuring the output), and the actuator positions are linked to the physical orientation of the heliostat mirror. The accuracy of an open loop-controlled heliostat can be increased by increasing the calibration interval and with the implementation of an error model. However, calibration requires the sunspot to move out of the high flux region of the receiver for it to be identified. The time a heliostat is not focussed on the receiver is wasted solar radiation. The calibration of a heliostat can be completed in variety of ways and it is an active field of research, later discussed in the following chapter. Both the open and closed loop heliostat control strategies will be discussed in depth, as well as control strategies incorporating a combination of open and closed loop control in an attempt to compensate for various tracking errors.

1.4 Helio40 facility

The Solar Thermal Energy Research Group (STERG) upgraded its solar roof laboratory in 2014 with the addition of an internally developed 40 m² (proposed aperture) heliostat test facility (Larmuth, et al., 2014). A photo of the facility is shown on Figure 6, consisting of two rows of control room roof mounted heliostats and 6 pedestal mounted heliostats. The tower is 18m high, with a calibration target mounted below the receiver.

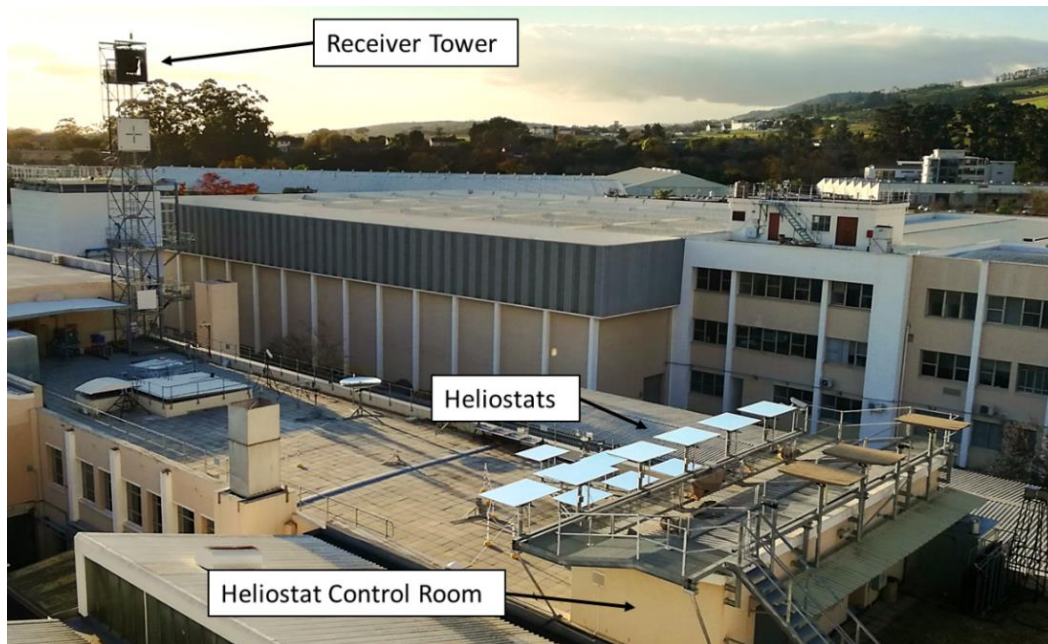


Figure 6: Photo of the heliostat facility, part of the Solar Thermal Energy Research Group (STERG) high temperature laboratory, located on the roof of the mechanical engineering building at Stellenbosch University.

The primary objective of the Helio40 facility was to develop a wireless control system with a model based open-loop error correction method to minimize deterministic tracking errors. The research also identified technology improvement opportunities to reduce the cost of the heliostat field, which typically makes up 40-50 per cent of a CRS plant's total cost (Larmuth, et al., 2014).

After the Helio40 facility was completed, focus shifted towards the Helio100 project (a unique heliostat technology developed by the Solar Thermal Energy Research Group (STERG) at Stellenbosch University, based on the experience gained from the Helio40 and previous projects). Construction of the Helio100 pilot facility was finished in late 2015, and the facility remained operational until late 2016 (Helio100, [S.a.]).

STERG's Helio40 facility was built as an engineering exercise, and only a few control system validation tracking tests were carried out at the high temperature roof laboratory. After focus shifted to the Helio100 project, the facility was left standing, and was not officially handed over as a fully functional asset for STERG's high temperature solar roof laboratory. The Helio40 facility soon became unserviceable as the various electronic components suffered water damage (refer to chapter 3 where this is documented). Moreover, the facility was also never used to conduct thermal receiver research utilizing the concentrated solar radiation of all the heliostats.

1.5 Objectives

The main objective of this research project is to recommission the Helio40 facility to be robust and easy to operate, so that it can be a functional asset of STERG's high temperature laboratory located on the roof of the mechanical engineering building at Stellenbosch University.

The graphical user interface (GUI) that is used to control the facility, and how it is accessed is a central focus of the project, as it will determine how user friendly and robust the recommissioned facility will be. The facility will need to be user friendly, as it will continually have new operators in the research environment. Further, the recommissioning should include all the necessary mechanical and electrical maintenance/replacement of components to get the hardware of the facility back in a reliable working condition. In the end of the project the Helio40 facility should be a functional tool of STERG's high temperature roof laboratory, that can be used for future CSP research.

This project represents a continuation of heliostat control systems research at STERG. However, the objectives differ to some extent compared to the work done previously on the Helio40 facility due to the following reasons:

- Focus will be shifted to tailor the control system specifically for the Helio40 facility, which will be used as a tool for CSP research.
- The facility is small, therefore the level of automation required for the control system does not resemble that of a commercial central receiver power plant with thousands of heliostats.
- The facility will only be used a few times annually, which removes the need for error propagation methods that aim to compensate for heliostat drift over long periods of time.
- The facility will not have a dedicated operator in the research environment.
- As the facility will be used for research projects that are generally time restricted, the facility will need to have a fast start-up and shutdown period.

The objectives of the project are:

- Use methods and practices during the recommissioning that ensures the robustness of the facility.
- Research different heliostat calibration and control methods.
- Develop and implement a calibration method that is best suited for the research facility .
- Develop, implement and test the heliostat control system
- Develop and implement a graphical user interface (GUI) which is accessible from the internet.
- Design the GUI to be simplistic and easy to use.

- Have the appropriate safety precautions incorporated into the hardware and programming, making it possible to respond to emergency situations.
- Concentrate work on the six pod-mounted heliostats and recommission the rest if time permits.

1.6 Methodology

Following from the objectives, the overall research methodology is summarized as:

- Review relevant literature and gain an understanding of the previous work done in the field.
- Decide on a control method to implement and test.
- Evaluate chosen control method and compare to system requirements.
- Design and implement the GUI and control system for the facility.
- Perform tests to evaluate system functionality and ease of use.

1.7 Scope and limitations

The nature of the project required a range of disciplines to be covered which include:

- Control system design
- General mechanical maintenance
- Wi-Fi communication between different platforms
- Programming of embedded processors
- Software development across multiple platforms
- PCB design
- Electronic circuit design
- Problem solving across all the covered disciplines
- Integration of all the different aspects of the Helio40 facility to function as a system

The project's scope is limited to the control of heliostats and does not include any research or work on the collection of concentrated solar radiation. Further the characterization and measuring of error propagation of the heliostats was also limited.

2 Literature review

The following chapter reviews established literature to introduce ideas principles and concepts relevant to central receiver systems in general, before focusing on the in-depth research field of heliostat calibration and control strategies.

2.1 Defining the solar position relative to an observer

The accurate position of the sun relative to a solar collection device is essential for all CSP systems that require solar tracking. The solar position can either be calculated using solar position algorithms or be directly obtained with directional light sensors. The accurate predictability of the solar position calculated with solar position algorithms (discussed in the following section) has made it the industry standard method of obtaining the solar vector CSP plants. However, for small independent collection devices or tracking PV systems, directional light sensors are commonly used.

The position of the sun is defined by two angles relative to the conventional earth-surface based coordinates which consist of a vertical line straight up (Zenith) and a horizontal plane containing a north-south line and an east-west line. These two angles are the solar altitude angle(α), which the central ray of the sun makes with the horizontal plane, and the solar azimuth angle(A), measured clockwise on the horizontal plane, from the north-pointing coordinate axis to the projection of the sun's central ray, as seen on Figure 7 below. Stine & Geyer's online available book "Power from the sun" discusses and presents the derivation of these angles in detail along with the established sun earth geometry.

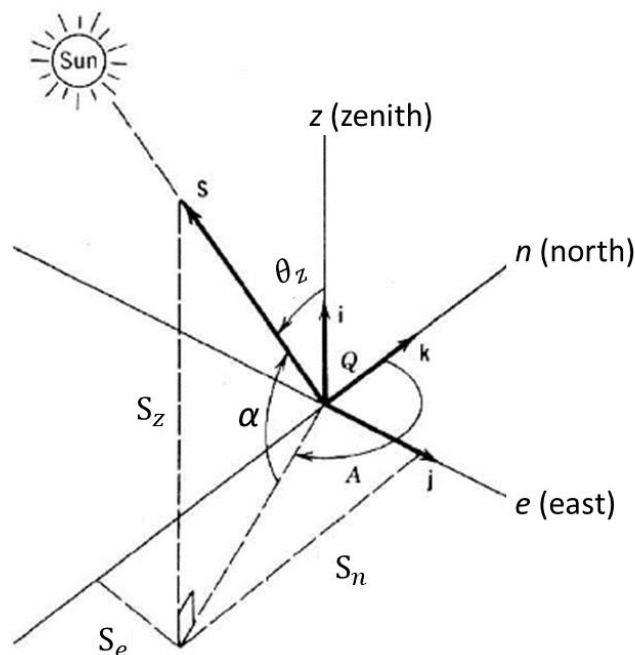


Figure 7: Earth surface coordinate system for observer at Q showing the solar azimuth angle A , the solar altitude angle (α) and the solar zenith angle (θ_z) for a central ray along direction vector S . (Source: Stine & Geyer 2001)

The earth's rotation causes the solar position to constantly change following a set path. The sun's path across the sky is commonly represented on 2D sun path diagrams. These diagrams are easy to use, however they only produce accuracies to within a few degrees. That said, on the internet (Marsh, 2014) a very intuitive and accurate 3D sun path simulation app is available. Marsh states that it was developed with the aim of demonstrating the relationship between geographic location and solar position throughout the year. The world map can be used to drag and select the observer location and interactively see how the Sun-path and rendered shadow projections change. The application also allows users to upload their own 3D CAD models to be simulated. Screenshots of the 3D sun path models are shown in Figure 8 below.

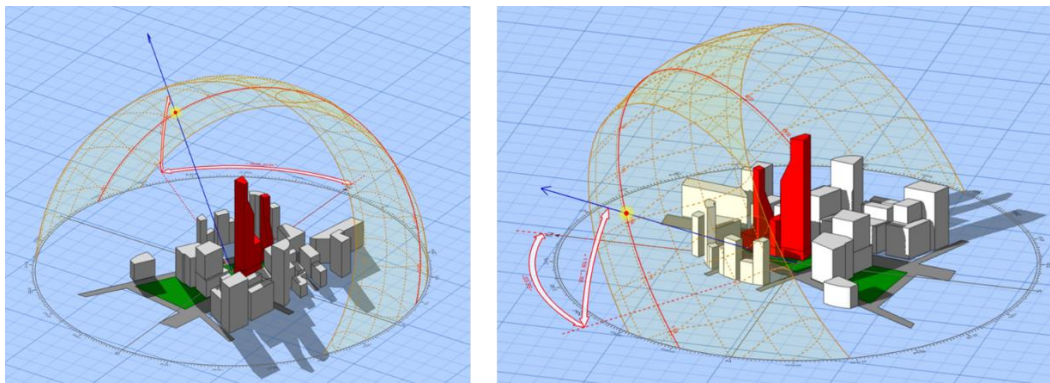


Figure 8: 3D Model showing the annual sun path of Stellenbosch (Source: Marsh, 2014)

Note that in Figure 8 the blue arrow represents the solar vector, and the red line lying on the yellow band enclosing the 3D buildings represents the solar path for the chosen day. An interesting observation made while interacting with the app is that at 8:20 in the morning, during the longest day in Stellenbosch (summer solstice), the sun is at the same altitude angle during solar noon for the shortest day of the year (winter solstice).

Solar position algorithms

Sun path diagrams and the online app shown previously are created using the output of solar position algorithms. These algorithms have increased in complexity over time by taking more variables into account to achieve higher angular certainty of the solar position. This trend is consequently due to the increasing computational abilities of computers over time following Moore's law, which states that the number of transistors in a dense integrated circuit doubles about every two years.

Cooper (1969), Spencer (1971), Swift (1976) and Lamm (1981) presented a few of the earlier algorithms with angular uncertainties in the tenths of degrees range. To date, the Solar Position Algorithm (SPA) by Reda and Andreas (2008) is by far the most accurate, with a maximum angular uncertainty of 0.0003 degrees. For all practical heliostat tracking applications, the precision of the (SPA) and ample computing power of modern computers has made the acquisition of the solar

position a hurdle that has been overcome, and consequently CSP research has focussed on compensating and reducing heliostat error sources rather than reducing solar position uncertainties.

2.2 Heliostat optics

The law of reflection states that the angle of incidence equals the angle of reflection, with the incident ray, the reflected ray and the normal vector of the mirror all lying in the same plane. This law explains how a heliostat must be oriented to reflect sunlight onto the receiver, where the incident ray is the central solar ray and the reflected ray is the fixed vector pointing towards the receiver from the centre of the heliostat mirror. Thus, as the sun moves across the sky, the heliostat is periodically updating its altitude and azimuth angles (vector H) to satisfy this condition, illustrated on Figure 9.

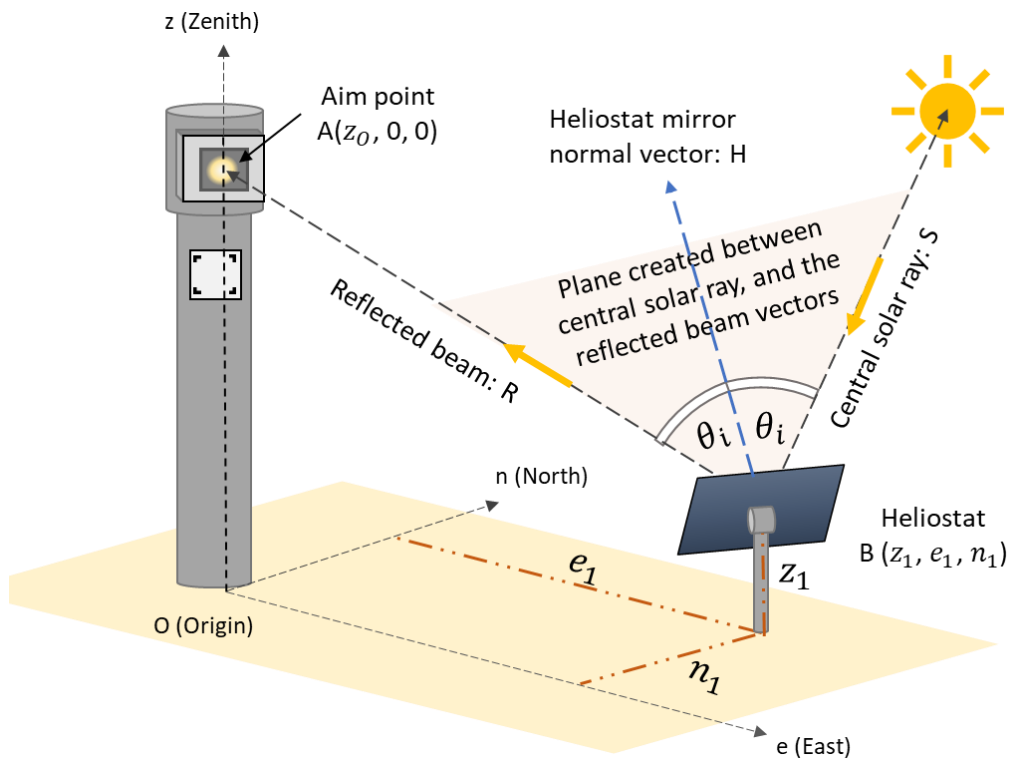


Figure 9: Heliostat optics

The vector H that needs to be calculated every time before a position update occurs is presented in equation 2.1 below.

$$H = \frac{R+S}{2\cos\theta_i} \quad (2.1)$$

Further, the heliostat pointing vector H can be described by the altitude and azimuth angles of the reflecting surface (α_H) and (A_H) respectively, in terms of the orthogonal coordinates presented in equation 2.2 and 2.3 respectively.

$$\sin \alpha_H = \frac{R_z + s \sin \alpha}{2\cos\theta_i} \quad (2.2)$$

$$\sin A_H = \frac{R_e + \cos \alpha \sin A}{2 \cos \theta_i} \quad (2.3)$$

Since the heliostats of the Helio40 facility are of the azimuth elevation design. The tracking updates or a position move will require that both equations 2.2 and 2.3 be solved, converted into encoder step counts and the actuation to the azimuth and altitude actuators until the respective calculated encoder positions are reached.

2.3 Heliostat tracking error

A heliostat tracking error is present when the reflected beam centroid is not intersecting the intended aimpoint position. More specifically, for open loop-controlled heliostats, the error is the difference in angle between the physical reflected beam, and the vector of the calculated beam angle in the control system, typically defined by actuator encoder values. Figure 10 illustrates this error.

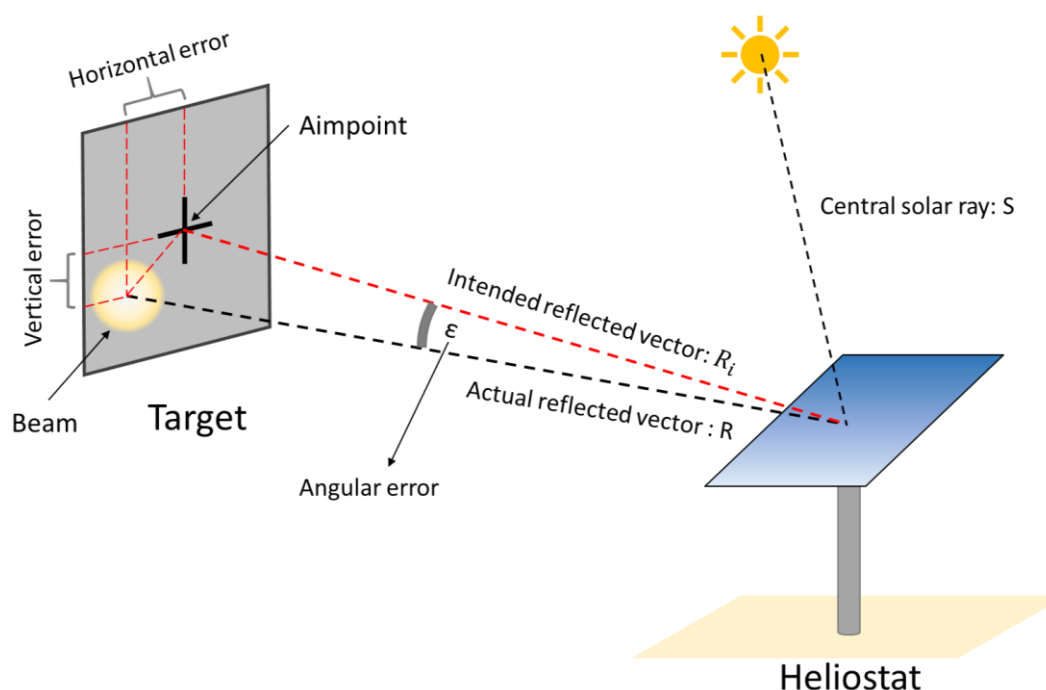


Figure 10: Heliostat tracking error

Tracking errors are primarily caused by subtle misalignments of the heliostat structure that tend to increase over time, that are not accounted for in the control system. These misalignments cause tracking errors which change throughout the day and year due to their non-linear dependence on the intended pointing vectors (Khalsa, et al., 2011). The research that contributed to the understanding and characterization of all the possible error causing factors that are present in a heliostat field has been driven by the fact that CSP plants usually have good thermal to electric conversion efficiencies, but under predicted energy collection from the heliostat field, which is a result of large heliostat tracking errors. (Stone & Jones, 1999) observed this fact and stated that these time-variant errors

plagued the Solar Two project, with solar energy collection from the heliostat field being 10-20% lower than expected.

Categorization of tracking error sources

Up to now, only the physical geometrical misalignment of a heliostat has been pointed out as an error causing source, however a heliostat's achievable pointing accuracy is primarily constrained by its design. (Freeman, et al., 2014) wrote a paper where various types of errors were identified, categorized and assessed based on their potential impact and level of difficulty of resolution. However, no distinct classification was made between the inherent design error (allowable tolerance) and errors that tend to increase over time until they fall outside design specification (causing problems). Freeman states that his study should be used merely as a guide to help solar engineers make design choices regarding the control and calibration systems of a central receiver power plant.

Inherent design tracking error

Tables 1 and 2 were created using some input from Freeman's paper and findings that are perpetuated in literature. Table 1 lists the design choices that determine the heliostat's inherent pointing accuracy. This accuracy is also referred to as the theoretical accuracy, and it cannot be increased with software or clever control strategies. In practice a heliostat will always have a pointing accuracy that is slightly worse than the theoretical, due to the host of physical misalignment errors that arise in the practical implementation of a design. However, if a heliostat is manufactured, assembled and installed in the field following all the design specifications it should produce a pointing accuracy that falls inside the acceptable design tolerance. If this is found not to be the case, the design engineers should revise the calculations made during the design process or invest in more prototype testing to validate design choices.

Table 1: Heliostat design choices that determine theoretical heliostat pointing accuracy

Fundamental design choices	Associated errors
Type of actuators	<ul style="list-style-type: none"> • Actuator backlash • Actuator back-drive • Actuator's positional accuracy
Heliostat structural design	<ul style="list-style-type: none"> • Structural deformation • Structural stiffness

The designers of a plant will specify the required design tolerance of the heliostat field, based on the receiver size, the distance between the heliostats and the receiver, and the receiver flux distribution requirements, which all form part of a big optimization problem to minimize the levelized cost of electricity (LCOE). (Baheti & Scott, 1980) stated that as a consensus, to minimize the spillage (irradiation missing the receiver), the allowable pointing error (pointing accuracy)

for large heliostat fields should not exceed 0.1 degrees (approximately 1,75 milliradians).

Misalignment errors that increase over time

The change of misalignment errors over time is a very undesirable trait of heliostat fields. (Mavis, 1988) was among the first researchers who observed that specifically pedestal tilt and orthogonality errors tend to increase after the installation and levelling of the heliostat field. The above was pointed out in his study from 1981 to 1986 that characterized the heliostat beam and tracking performance of the 10 MWe Solar One central receiver pilot plant.

The three main misalignment errors that tend to increase after the commissioning of a plant is defined below, followed by Table 2 that lists these errors and the factors which cause them.

Pedestal tilt is present when the rotational axis of the azimuth actuator is not normal to the horizontal plane. Although the error is commonly described as the tilt of the physical pedestal, the error is dependent on the orientation of the rotational axis, that is not necessarily the same as the pedestal.

Boresight error or canting error is introduced when the heliostat facets are canted to focus along an optical axis that deviates from the pointing vector defined by the drive-axes.

Non-perpendicular rotational axes, as the name implies, refer to the azimuth and elevation rotating axes not being perpendicular.

Table 2: Heliostat misalignment errors

	Misalignment error	As a result of	Factors
Tracking error	Pedestal tilt	<ul style="list-style-type: none"> • Foundation settling • Structural creep • Structural yielding 	<ul style="list-style-type: none"> • Gravitational effects • Wind Loading • Thermal expansion & contraction • Soil properties • Rainfall
	Boresight error (also commonly referred to as canting error)	<ul style="list-style-type: none"> • Structural creep • Structural yielding 	<ul style="list-style-type: none"> • Wind Loading • Thermal expansion & contraction • Gravitational effects
	Non-perpendicular rotational axes	<ul style="list-style-type: none"> • Structural creep • Structural yielding 	<ul style="list-style-type: none"> • Wind Loading • Thermal expansion & contraction • Gravitational effects

The interaction between all the factors listed in Table 2, make it practically impossible to predict the development of misalignment errors. For example, a combination of rainfall, constant high wind speeds and a variation of soil properties throughout the heliostat field can cause pedestal tilt errors that are different for each individual heliostat. Moreover, sudden gusts of wind may cause structural yielding of some heliostats, leading to either a boresight error or non-perpendicular rotational axes.

Only closed loop and model based open loop tracking methods are able to account for these ever-changing misalignment errors. Closed loop tracking can account for basically any external disturbance, while model based open loop tracking will require a certain amount of calibration data to correctly identify the type of misalignment, its severity and its orientation. Thus, for model based open loop tracking to be effective, the model variables attained from a calibration, should produce accurate tracking up to the point when the next calibration is due. These periods between consecutive calibration, must be kept as short as possible, as the misalignments errors are inevitably changing over time. This puts a lot of strain on the control system as central receiver plants tend to have thousands of heliostats.

Another way to try and account for these errors is to increase the stiffness of the heliostat structure and increase size & depth of the foundations. However, this is not economically viable, as the heliostat field constitutes about 50% of the total capital cost of a CRS power plant, as stated by (Kolb et al. 2007) at Sandia National Labs, USA. This fact means there is an incentive for plant designers to decrease the cost of the heliostat field.

In an attempt to reduce the heliostat field cost, the Helio100 project (Helio100, [S.a.]) pursued the thinking to reduce design tolerances, remove foundations and ground preparation and deal with the associated increased misalignment errors (and the rate of change of these errors) by implementing model based open loop tracking. Although cost savings can be made by relaxing these geometrical alignment specifications, the theoretical achievable pointing accuracy requirement mentioned earlier (dependent on the actuators and the heliostat's structural stiffness), will always have to be fulfilled.

2.4 Heliostat control strategies

Since the early stages of CRS development, various calibration and control strategies have been developed, presented in literature and tested in the field to assess their tracking performance. This section reviews these different heliostat control strategies.

2.4.1 Classification of control strategies

Figure 11 was created to illustrate the different classification of control strategies, where the open and closed loop strategies are the two main subdivisions.

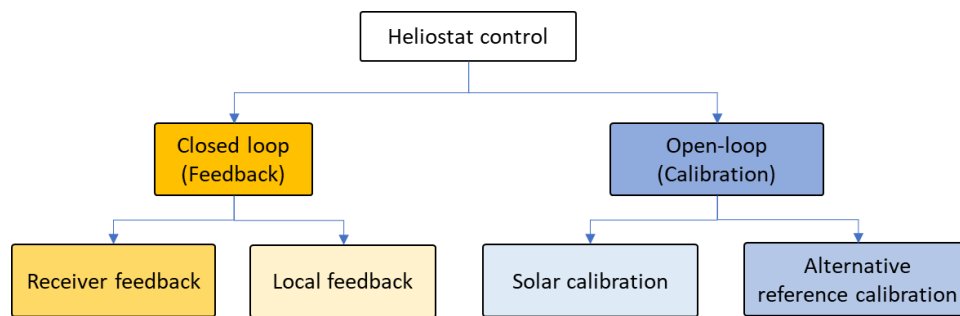


Figure 11: Heliostat control strategies classification

It should be noted that the closed loop-controlled heliostats typically still utilize some degree of actuator feedback (open loop control), as the heliostats still need to defocus, stow and refocus, that can only be accomplished with actuator position feedback (typically rotary encoders).

2.4.2 Closed loop control

Closed loop control of heliostats can be subdivided into receiver and local feedback. This classification, as the name implies, refers to where the output is measured.

Closed loop control with receiver feedback

A method of closed loop control using cameras located around the receiver aperture is described in a patent application by (Yogev & Krupin, 1999). The idea is that 4 cameras located above, below and on either side of the receiver look back at the field, each identifying the individual heliostats and assessing their brightness. As tracking commences, images of opposing cameras are compared, and misaligned heliostats can be identified due to the brightness imbalance on the two images. The control system then uses this information to correct the misaligned heliostats until all brightness imbalances are eliminated. It should be noted that this methodology is used in combination with regular open loop control, requiring actuators with internal position feedback to stow, defocus and refocus heliostats, as no usable feedback is produced from the images taken by the cameras if the heliostats are reflecting away from the aperture.

(Kribus, et al., 2004) published their work where a system based on the Yogev and Krupkin patent is successfully implemented, at the Weizmann Institute's heliostat field in Tel Aviv. The results show that individual heliostat tracking errors were reduced to 0.1 - 0.3 milliradians, equivalent to about 50 mm of beam movement on the facility's receiver. The authors of the research recommend that this method should be considered for commercial scale heliostat fields, however, to date this system has not been implemented on a commercial CRS plant, mostly attributed to problems associated with operating cameras close to a high flux thermal receiver. Furthermore, the Weizmann institute where the system was developed and operated has a south facing heliostat field, with an aperture receiver design, which is well suited to accommodate the mounting of cameras around the receiver opening. The trend of commercial CRS however, is to have a

central cylindrical receiver that is irradiated radially around its circumference. Thus, for the system to be implemented on a central tower, the receiver design would have to be a segmented multiple aperture receiver to accommodate the mounting of cameras around the individual apertures, as illustrated on Figure 12. This system could therefore be implemented on the Helio40 facility, but as experimental receivers will be added and removed in the research environment it would be better to not have the control system dependent on hardware mounted on a temporary receiver.

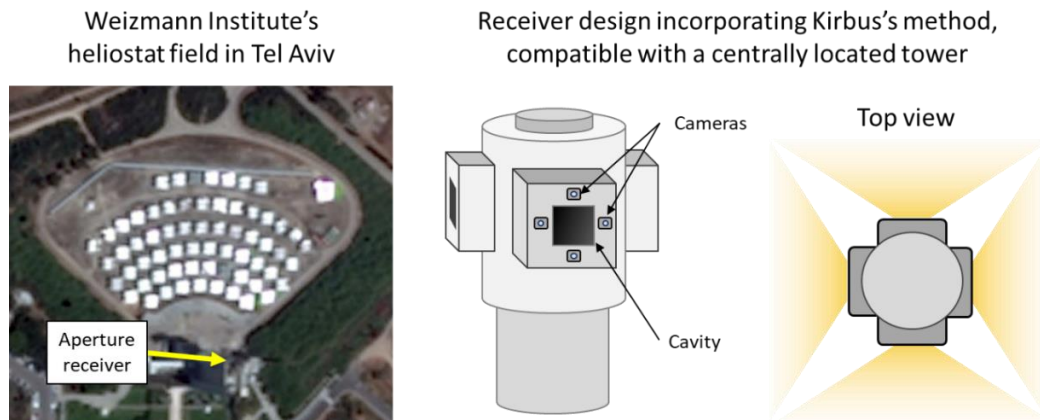


Figure 12: Satellite image of the Weizmann institutes heliostat field, as well as a receiver design that uses Kribus's method and accepts concentrated radiation all around its circumference.

Another novel method of closing the control loop is described by (Convery, 2011). The operating principle is similar to the method described previously, however, four photodiodes are mounted around the receiver instead of cameras. Photodiodes alone can only detect a change in light intensity, thus to be able to identify an individual heliostat reflection, piezoelectric actuators are mounted to the mirrors of all the heliostats to induce vibrations and modulate the reflected sunlight with a unique frequency. The heliostat specific frequency is then detected by the photodiodes, identifying the corresponding heliostat. As stated, the method requires the addition of more hardware (piezoelectric actuators) installed in the field, however the control system does not require the computational expensive digital image processing required by the former method. Furthermore, photodiodes are more robust than CCD cameras (due to their simple construction and working principle) and would be easier to protect against the high solar flux and elevated temperatures present around a thermal receiver. This methodology has only been tested on a small experimental scale and is also constrained to cavity/planar receivers as discussed previously.

(Bern, et al., 2017) describes an approach aimed at the extraction of heliostat focal spot positions within the receiver domain by means of a camera system looking at the receiver, away from the rough conditions close to the focal area. The approach is similar to that of Convery with regards to identifying focal spots using modulated frequencies, albeit the driving frequency used is much lower (0.2 to 2 Hz instead

of the kilohertz audio frequency range used by Convery. The slow movements allow for the utilization of the heliostat actuators to modulate the reflected sunlight instead of adding additional hardware, cabling and I/O- infrastructure to each heliostat. This makes the control strategy easy to deploy in existing plants. The authors did mention that the selection of the driving frequency should be carefully selected, as wind-induced vibrations and resonant frequencies of structures may compromise the original driving frequency. Additionally, the effect of an unequal amount of backlash present in heliostat actuators should also be investigated, as well as the affect the orientation of the heliostat has on the output of the driving frequency. The authors state that the strategy has been tested with full scale heliostats and the Mini-Pegase-Receiver, motivating further investigation and deployment.

(Goldberg, et al., 2015) (a senior director at BrightSource Industries) describes embedding a visual range camera inside a solar receiver gazing back at the field, in an attempt to measure how much energy each heliostat contributes at all times, and at what part of the receiver it aims. The camera can withstand the high solar flux, thanks to active cooling and its pinhole design which serves the same function of an eye's iris that contracts (decreasing the amount of light entering the eye and hitting the retina) when exposed to bright light. The paper states that the pinhole camera was successfully tested at the BrightSource Solar Energy Development Centre (SEDC) over a period of two years, and that details of individual heliostats are readily visible on the obtained images. The applications of this methodology are extremely broad, ranging from the better estimation of expected flux maps, heliostat tracking error correction, shortening solar field maintenance tasks such as fast detection of dirty or broken mirrors, etc. The work done in the paper is very interesting, as it describes how the pinhole camera can be used to better integrate the control of the heliostat field with the control of the receiver and improve efficiency and the reliable operation of the plant.

Closed loop control with local heliostat feedback

Local feedback refers to obtaining feedback further down the control path from the reflected beam somewhere between the field and receiver, or the physical orientation of the mirror which eliminates a lot of errors but requires additional sensors in the field typically for each individual heliostat. These sensors are also not immune to calibration.

(Quero, et al., 2007) developed a microelectromechanical (MEM) incident light angle sensor for application in a heliostat field to retrieve feedback from the reflected heliostat beam. The sensor is placed in between the heliostat and tower as seen on Figure 13, and generates an alignment error signal, which is used to control the heliostat's movements.

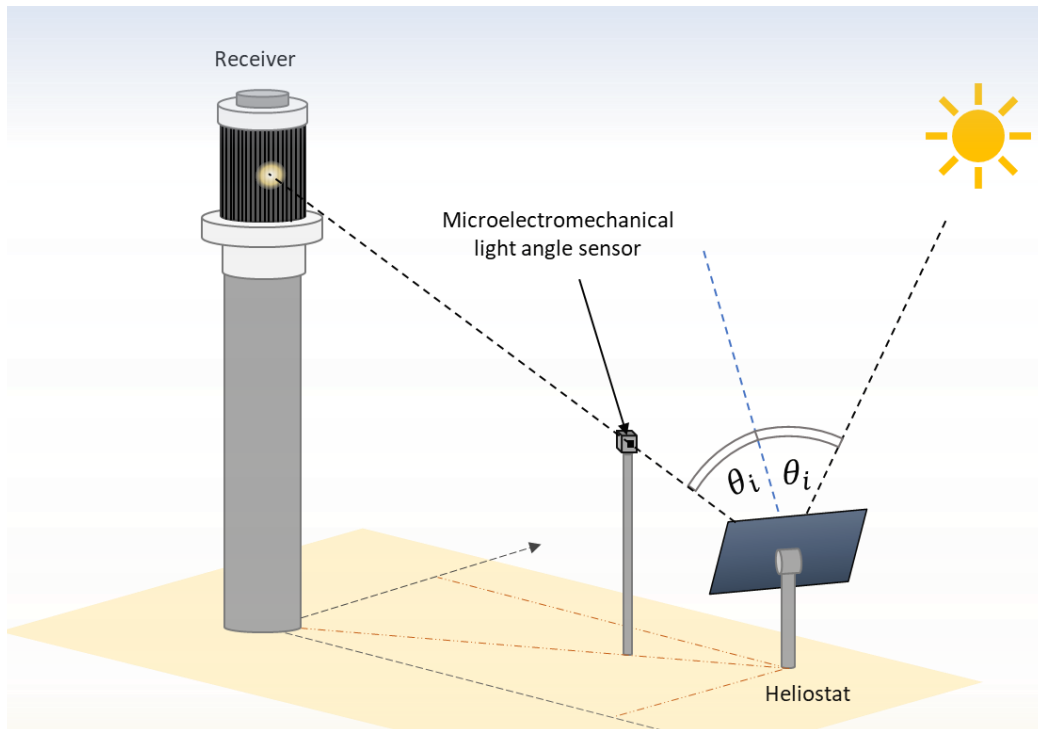


Figure 13: Local feedback from incident light angle sensor located between target and facet

These sensors do require an initial calibration, and the structure they are mounted to needs to be rigid, as movement of the sensor due to wind or foundation sag will introduce new errors into the control loop defeating the purpose of control strategy. The authors state that the system has been implemented and tested, which revealed one unforeseen problem that arises when the reflection of the sunray changed from one facet to another (an industry standard heliostat normally has multiple facets). The authors solved this problem by placing more sensors working in parallel, and by including a comparison strategy in their error signal. This solution does require the addition of more sensors which is not ideal, and the problem only appeared during the physical testing of the proposed method, which highlights the absolute importance for new concepts and ideas to be physically tested in the field before any valid claims can be made. The authors state that an accuracy of 1 milliradians was achieved during testing of the system, where the accuracy can be increased by moving the sensor closer to the receiver. It should be noted that the sensor is heliostat specific and the distance from the heliostat is limited to the point where neighbouring heliostat beams start merging with the measured beam, as illustrated on Figure 14.

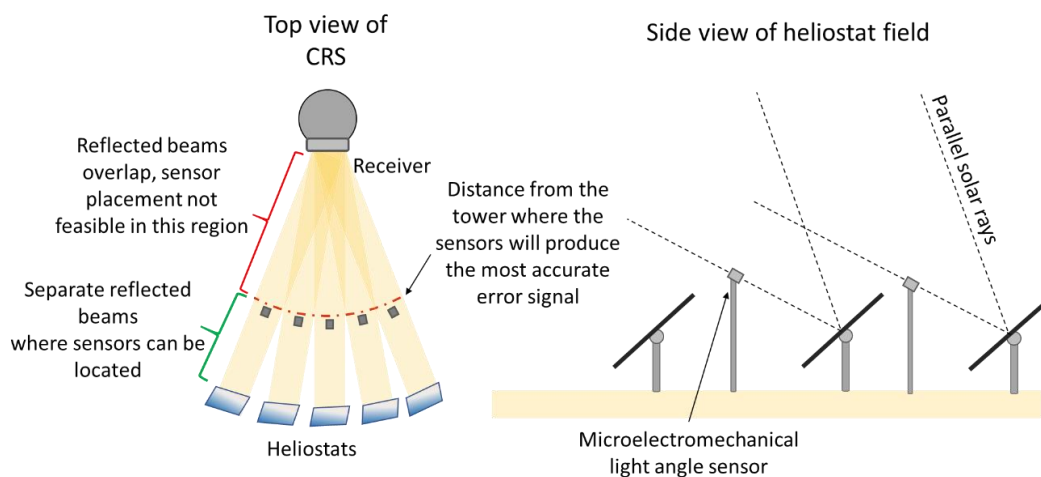


Figure 14: Top view of a CRS plant showing the limitations of sensor placement

(Roos, 2009) designed, built and tested a 25m² target-aligned research heliostat at CSIR in South Africa, with a control system making use of a solar tracker. The solar tracker protrudes from a hole in the middle of the facet and is actuated to track the sun through a 2:1 mechanical gearing that is connected to the heliostat facet. This design is not a true closed loop system as the output is not measured, however no calculation of sun angles is necessary as the tracking is completely autonomous. The accuracy of a heliostat incorporating this type of tracking mechanism depends greatly on the precision of the mechanical gearing between the solar tracker and heliostat facet and also the achievable accuracy of the solar tracking sensor, and its initial calibration. The author states that the research heliostat produced a tracking accuracy of 3.3 milliradians. This is not very accurate compared to modern industrial heliostats, but the fact that it is the maximum error is significant. The heliostat Roos designed and built is unique and has not been adopted by industry, most probably due to the rather complex mechanical design.

2.4.3 Open loop control

Open loop-controlled heliostats have potential error sources from the encoders (generally mounted on the actuator's motor axis for high resolution) all the way down the control path to the output which is the position of the reflected solar image on the receiver.

Open loop control employing solar calibration

In a patent application by (Stone, 1986) a comprehensive method is described of automatically aligning heliostats by comparing the actual sunbeam centroid position on a target to a command reference position (usually the centre of the target) to determine the sunbeam position error. The idea is that a camera is aimed at the offset correction target which is generally mounted below the receiver (illustrated in Figure 15), and a central computer automatically commands heliostats to reflect onto the target while the sunspot is identified, and the error is measured and corrected. Stone states that the process should be completed periodically for each heliostat to collect enough data to make the

necessary alignment calculations. The core principle of this methodology has since become a very common calibration method of open loop-controlled heliostats, as it requires no additional hardware in the field, other than a camera and a target mounted to the tower, typically below the receiver.

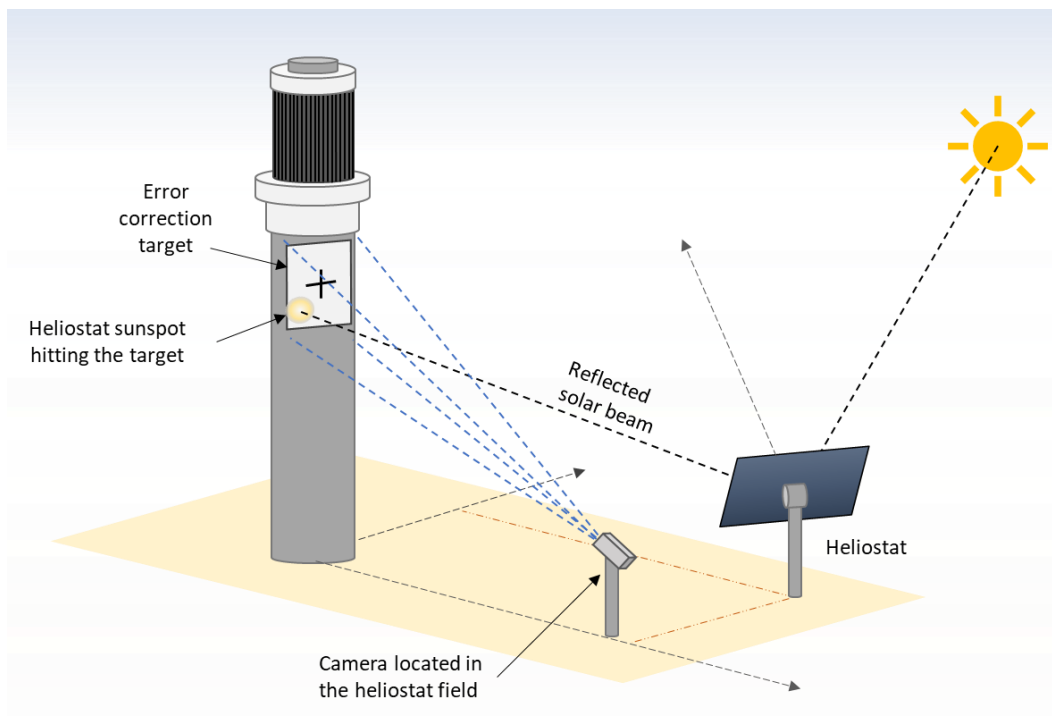


Figure 15: Heliostat calibration incorporating an error correction target

Based on the method described by Stone, (Berenguel, et al., 2004) presents the development of a simplified and automatic heliostat positioning offset correction control system using common CCD cameras. The developed software tool was successfully tested at the CESA-1 plant at the Plataforma Solar de Almería (south east Spain) where the objective to replace the operators of the plant who at the time manually performed the offset corrections was achieved. The authors state that for small-scale installations the presented algorithm works well, and operators only have to perform the supervision of the process, however for large-scale plants, modifications are required in the direction of the development of more complete and accurate systems, such as the beam characterization system (BCS) developed for Solar One (see references).

(Iriarte-cornejo, et al., 2014) developed a heuristic dynamic compensation method for heliostat drift based on third degree polynomial functions of time. The method aims to be an improvement to the error-correcting model implemented by (Stone & Jones, 1999) at “Solar Two” that also eliminates time variant tracking errors but requires many tracking accuracy measurements over a day to calculate the magnitude of each error source. The authors state that about 40 heliostats could be calibrated per day, with the method being tested experimentally for 10 heliostats with good short-term results, and that only numerical simulations have been carried out to validate the method for a year of operation. The authors also

claim that the averaged (RMSD) root mean square deviation of the sun spot location at the receiver is reduced to 39% of its original value for the different cases tested.

(Malan, 2014) developed a scalable, modular and adaptable control system incorporating model based open-loop error correction, intended for low cost heliostats. The method is based on the work done by Baheti & Scott and Stone in the 1980's and recently (Khalsa, et al., 2011). The error model differs from that of Khalsa, Ho and Andraka in that it includes a translation step to account for heliostat location uncertainty resulting from deployment of heliostats on rough terrain. The tracking method is therefore responsible for correcting tracking errors associated with very low installation and manufacturing tolerances, placing a lot responsibility on the control system to account for all the alignment errors. The author state that more experimental data should be gathered at different times of year in order to refine the model and achieve better understanding of its sensitivity to a change in parameters. The Helio40 and Helio100 projects that was based on the work of the author, inherited the same philosophy, sparking a few articles in CSP development. After funding for these projects ended, the facilities were not used anymore.

The characterization and correction of heliostat errors using error models is an attractive research field and the current industry trend as it can dramatically improve tracking accuracy, increasing plant efficiency with little to no additional capital investment. These methods require extensive long-term tests to validate the theoretical results, as it is the only way to account for seasonal changes of the sun path which affects tracking dynamics. The method is also complicated as it tries to correct the misalignment errors (that produce time varying tracking errors) which tend to change over time as the heliostat structure and foundation settles, by using as little as possible snapshots of the beam error taken at different time intervals. Thus, it is essential to find the frequency of feedback intervals (calibration) that will ensure the tracking requirements are met while simultaneously being able to calibrate the entire field before the heliostats that were calibrated first, start having excessive tracking errors. In essence, it boils down to an optimization problem where the number of heliostats (heliostat field size), the rate of change of misalignment errors, tracking accuracy requirements and heliostat down time as a result of calibration are all factors that need to be taken into account when selecting a specific control method for a CRS plant.

Open loop control employing alternative reference calibration

Although calibration using the sun is the most accurate and widely used method, it restricts the process to only a few daylight hours. In an attempt to reduce the time needed for calibrating large fields, methods with references apart from the sun have been developed, such as the use of celestial bodies at night or the implementation of artificial illumination, as presented by (Schell, 2011) and (Zavodny, et al., 2015).

In the comprehensive study by (Mavis, 1988) of the Solar One 10 MWe CRS Pilot Plant that spanned from November 1981 - December 1986, the concept of “moontracking” is evaluated. The method uses moonlight as the light source and reflects it to an aim point below the receiver. Mavis states that an observer located at the aim point on the tower then identifies which heliostats have large tracking errors or misaligned mirrors, as illustrated of Figure 16. These heliostats can then be scheduled for maintenance and/or calibration to correct the errors. The moontracking method is thus only used to streamline the solar calibration and maintenance processes, similar to the method pointed out by Goldberg, without having to deal with the high solar flux. The method can easily be automated using the technology developed by traditional back gazing systems to improve its efficiency. The ability of moontracking to extract information from the heliostat field at night, and use it to improve the energy collection, makes it a valuable tool any CRS can add to their control toolbox. It should be noted that the method is dependent on the moon cycles, and cloud cover.

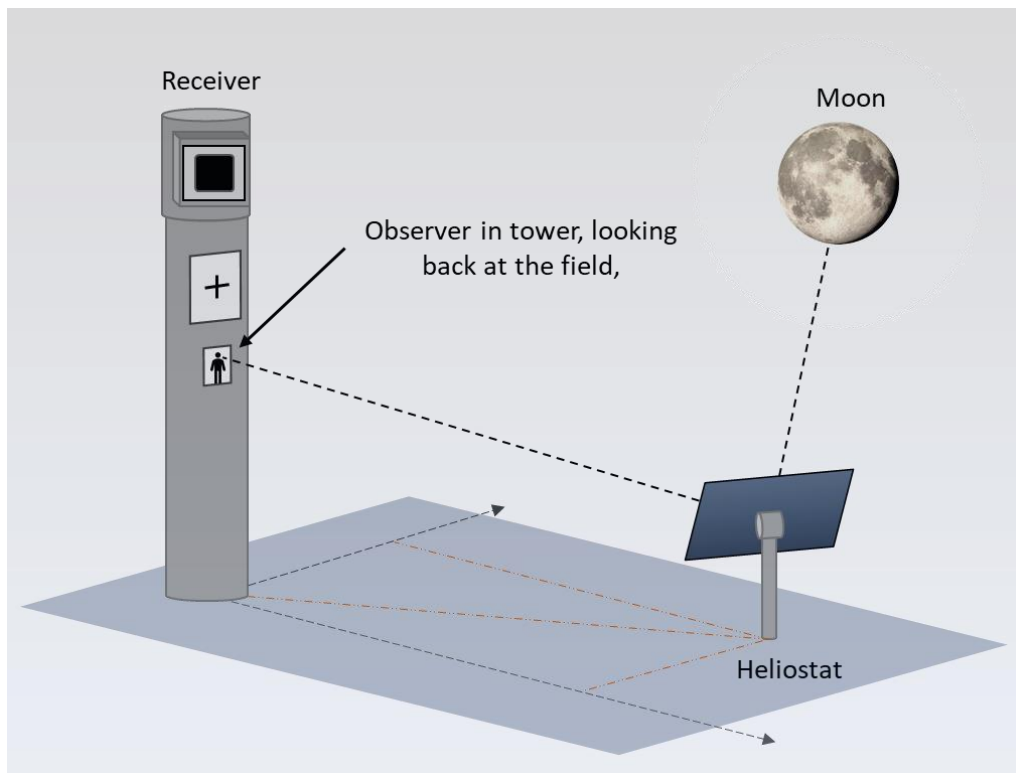


Figure 16: Moontracking method

(Zavodny, et al., 2015) describes the development of eSolar’s patented Artificial Light Calibration (ALC) method in a very interesting article. The ALC method was developed at eSolar's modular 5 MW CSP plant in Lancaster, California, which has been decommissioned since 2015 due to high operational costs. The method works by reflecting light from LEDs located on towers around the field into cameras, which are mounted to the same towers. The method is novel, as the calibration is performed during the night when the field is not in use for power production. Other calibration systems require that some percentage of the

available flux be diverted for calibration data collection, which can result in as much as 1-2% field availability loss. Further, the cameras can be sourced from many low-cost options as they are not subject to concentrated solar flux. This means that the whole field can reflect the artificial light to a single camera for calibration purposes. Another advantage of the system is that unlike the sun, the LED lights remain stationary as time passes. This enables the system to repeat the data collection event for any camera-light-heliostat as a double-check to estimate its own precision. The proximity of the lights and cameras to the field trumps solar calibration yet again, as cloud cover or even rain does not affect the calibration process. The one big challenge intrinsic to the ALC method is that the sun is not the reference for the calibration process. This opens the possibility for systematic errors to manifest themselves in the surveyed positions of the lights, cameras and heliostats relative to the global coordinate system where the sun position is defined. In the article, the author describes that this uncertainty is dealt with during the day time, when some heliostat reflections from the sun are gathered to validate that the global coordinate system defining the heliostat, camera, and light positions, is aligned with the coordinate system used to estimate the position of the sun during tracking.

3 Helio40 facility Inspection

3.1 Initial facility inspection

Upon first inspection of the facility, it was clear that the heliostats were not in working condition. A lot of condensation was present in some of the enclosures housing the control electronics, and the heliostat power switch board inside the control room was not working or connected to a power source. However, the actuators and general structure was in good condition with only fasteners showing signs of corrosion. Figure 17 below shows the extent of water damage to some of the electronic components.

Water damage of electrical components

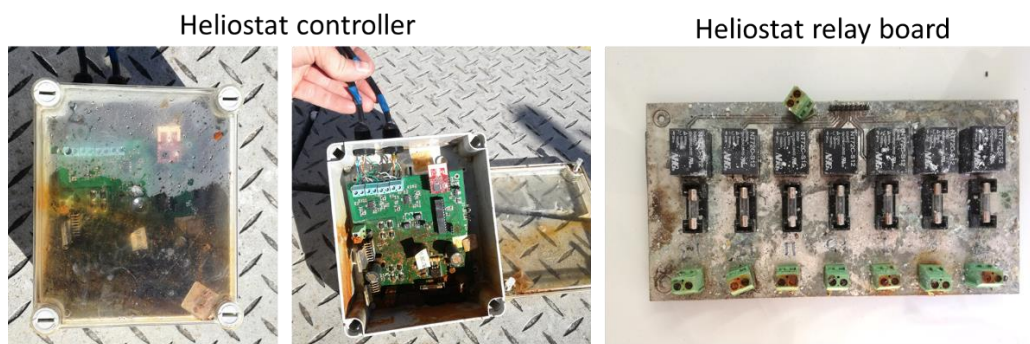


Figure 17: Water damage of a heliostat local controller (left) and the roof mounted power relay board (right) that distributes power to the individual local controllers.

After the initial inspection, all the actuators were tested with a 24-volt DC supply to ensure the motors and gearing were in a serviceable condition. The encoder output signals were also tested with a purpose-built LED encoder tester that switches two LED's on and off as the rotary incremental encoder rotates.

The tests revealed that most of the actuators were in working condition, with one linear actuator having a seized motor, and most of the slewing drives having noticeable backlash. The linear actuator was disassembled and repaired, while the backlash of the slewing drives is an inherent error that cannot be fixed with general maintenance. As stated earlier in section 2.3.1, actuator backlash is very undesirable since it is an error that cannot be compensated for in the control system, and it directly decreases the accuracy of a heliostat.

It was clear from first inspection that the facility was rapidly built as a prototype pilot facility. New designs and methods were applied and tested during its commissioning, with afterthought solutions visible throughout the facility. The electrical wiring inside the power switching board and local controller enclosures was chaotic, with little consideration for long term reliability or maintenance.

The inspection concluded that the heliostats needed new electronic control boards as well as a user interface from which the facility would be controlled.

Furthermore, a heliostat control program is also required, which could be tailored for the facility.

3.2 General system considerations

3.2.1 Tracking update frequency

When a properly designed heliostat without any misalignment errors is calibrated, its tracking accuracy, or the amount of sunspot movement across the receiver is determined by the tracking update frequency. As the sun moves across the sky at an angular velocity of 15 degrees per hour, the required update frequency can be easily calculated using the plant's receiver requirements. The Helio40 facility does not have a dedicated receiver, but rather serves as a platform where different receiver designs can be tested. For this reason, the update frequency will be adaptive, with an arbitrary default of 30 seconds. In 30 seconds, the sunspot will drift by only 0.1 meters on the receiver between each tracking update, with an average heliostat to receiver distance of 48 meters (Larmuth, et al., 2014). Figure 18 illustrates how much the centroid of the reflected sunbeam will move relative to the calibration target before a tracking update takes place. As a result of the south-east located collection field relative to the tower, the sunspots will always drift to the right side of the aimpoint as the sun moves across the sky (to the bottom right corner before noon, to the right during noon and to the top right in the afternoon).

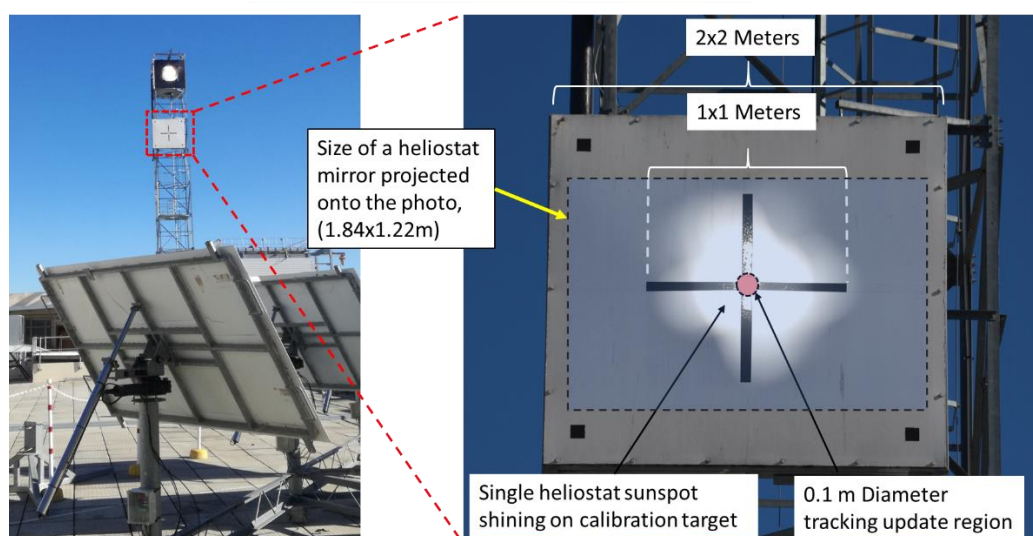


Figure 18: Illustration of sunspot movement with a 30 second tracking update interval.

Also shown on Figure 18, is the size of the heliostat facets projected onto the photo. It is clearly visible that the mirrors concentrate the solar radiation, with the sunspot on the target being roughly a quarter of the size of the mirror. Although the overall concentration ratio is approximately 4:1, the flux distribution of the sunspot reflected onto a flat surface will resemble a circular Gaussian distribution, as found by (Boese, et al., 1981). This property is visible on Figure 18, with the brightness increasing towards the centre of the sunspot.

3.2.2 Safety considerations

The proximity of the test facility to the neighbouring buildings is shown in a Google satellite image on Figure 20. The 47.5-meter focal length of the mirrors is overlaid onto the satellite image, and it is clear that safety precautions have to be implemented into the control system to prevent the heliostats from going out of control and shining onto the neighbouring buildings, potentially injuring unsuspecting individuals.

To assess the potential danger of a heliostat accidentally reflecting solar radiation at a person, the literature was reviewed. (Ho, et al., 2011) did a comprehensive study assessing the potential glint and glare hazards from concentrating solar power plants. Their work was used to predict if the Helio40 facility's heliostats can cause retinal burn (permanent damage to the eye). The authors state that the ocular safety metrics used to predict the potential for retinal burn were based on a 0.15 second exposure of the light source, as it is the average human blink reaction time. Figure 19 shows the calculated distances from a heliostat where potential retinal burn will occur, assuming a beam divergence angle of 9.4 milliradians (non-parallel solar rays), mirror reflectivity of 92 %, no mirror slope errors, solar insolation of 1000 W/m^2 and no cosine losses. These assumptions therefore represent the worst-case scenario concerning eye damage. Thus, the calculated critical zone shown on Figure 20 should be treated as the distance where permanent eye damage can theoretically occur. The operator of the facility must therefore be competent and remain vigilant while supervising the tracking of the heliostats to recognise possible control failures and act accordingly.

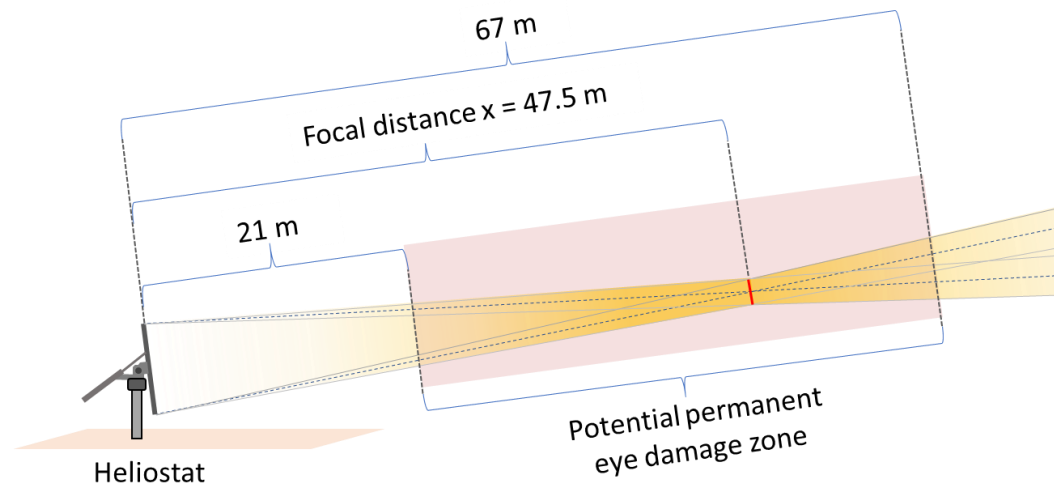


Figure 19: Heliostat potential permanent eye damage zone

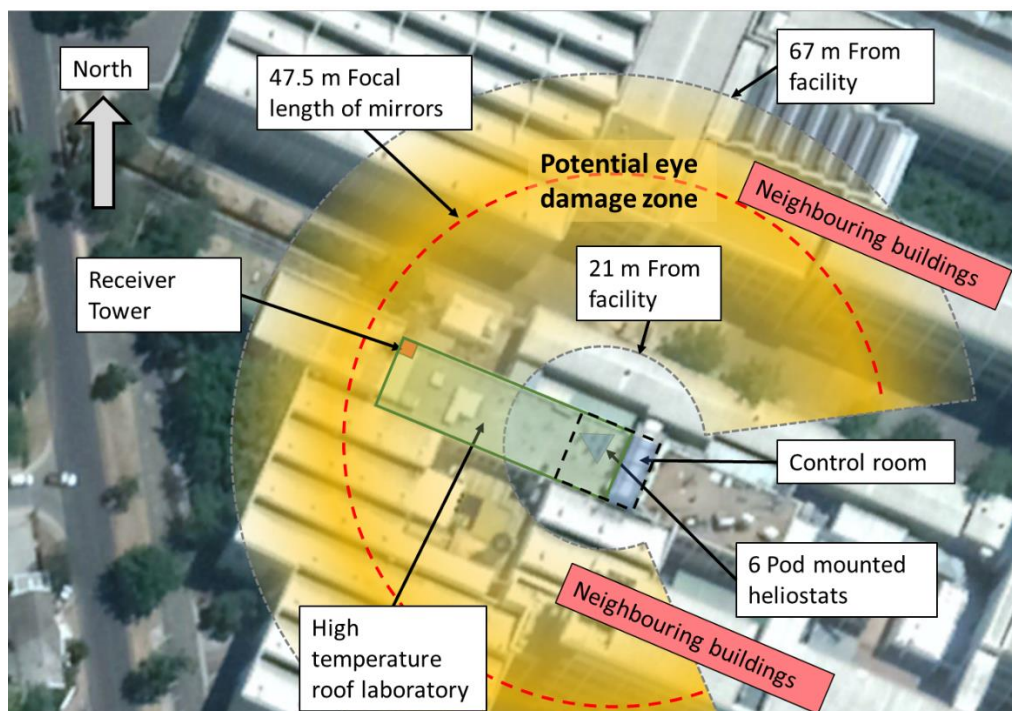


Figure 20: Satellite image of high temperature roof laboratory, showing the neighbouring buildings being within the potential eye damage zone.

4 Maintenance done on facility

Before the new controllers could be installed and tested on the pod, the power supply infrastructure and heliostat warning system had to be fixed. None of the systems were working and a substantial amount of time was spent checking connections, rerouting wires, soldering and testing the completed wiring.

4.1 Overhaul of electrical wiring

The power infrastructure of the facility has a tree structure, with only one main power cable leading from the switchboard in the control room to the relay distribution boxes on the pod, front, and back row roof heliostats. At the relay distribution boxes power cables branch out to the individual heliostats. The switchboard inside the control room has a toggle switch for each heliostat. When switched on, the small corresponding LED lights up on the panel, and the corresponding relay is switched on in the relay box through a signal wire. This design eliminates the need for power cables between each heliostat and the control room and allows each individual heliostat to be powered independently. Figure 21 shows the relay board as well as the heliostat switchboard after the overhaul. Notice that on the switchboard, heliostats 1 to 12 are switched on, indicated by the LED's, and on the relay box, LED's were added in parallel to the output of each channel, which serves as confirmation that the relays are working and that the fuse inside the distribution box is intact.

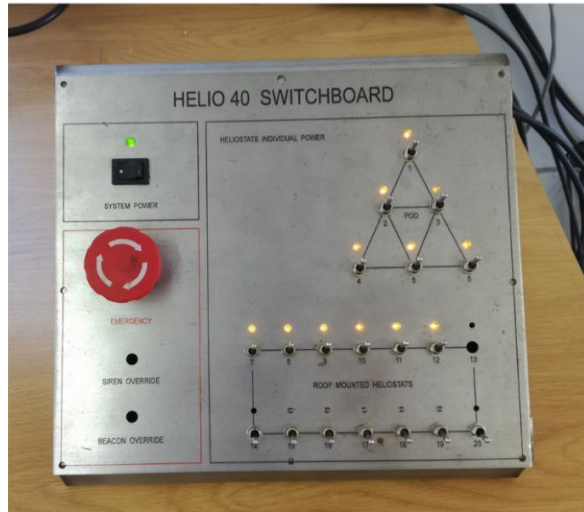
Helio40 pod relay power distribution box**Power Switchboard**

Figure 21: Relay distribution box (left) and the switchboard (right)

The wiring of the Switch box and pod relay board was completely overhauled, and care was taken to insulate all the solder connections with heat shrink tubing and add strain relief wherever possible using cable ties. The back of the switchboard panel is shown on Figure 22, before and after the wiring overhaul.

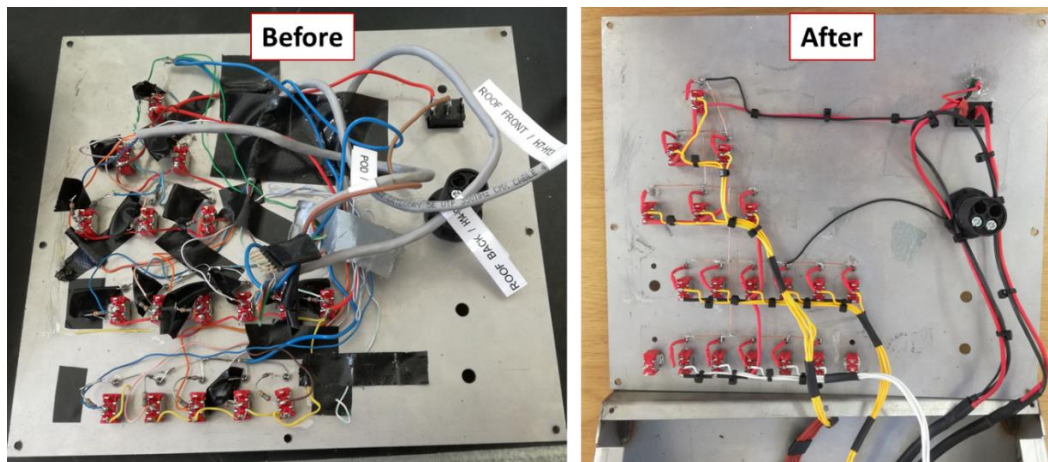


Figure 22: Rewiring of the switchboard

In addition, a UPS was added in between the grid power and the 24V DC power supply, providing power to the heliostats in case of a power failure. Figure 23 shows the layout of the heliostat pod power infrastructure.

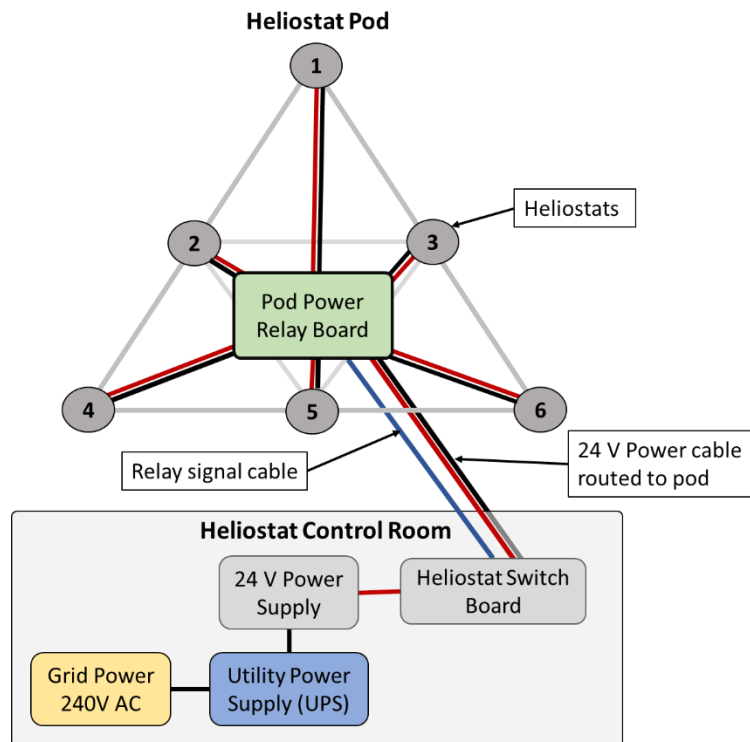


Figure 23: Heliostat Pod power infrastructure (roof mounted heliostats not included in illustration)

While the heliostats are in operation (system is powered), strobe lights turn on in the control room and the opposite office. In addition, there is also an alarm that activates when the door on the opposite office is opened. All the hardware for the warning system was already in place but not working. General maintenance was performed to get the system back to a serviceable condition.

4.2 Levelling of heliostat pod

Eliminating tracking errors by means of realigning the heliostats is not the general recommended procedure for central receiver power plants, since they consist of thousands of heliostats (time consuming) and as mentioned before, these errors tend to change over time. However, considering the size of the Heliostat facility and the fact that the heliostats are firmly secured on the solar roof, it is a viable option to increase tracking accuracy without implementing an error model.

The first tests that were carried out with heliostat number one, revealed that a small amount of sunspot drift was present (the first tracking tests are discussed in section 5.1.3). This drift is due to misalignment error sources that are not accounted for in the open loop control system. The most evident misalignment error present on the pod, was caused by the water drainage slope of the roof. Moreover, each heliostat had its own individual pedestal tilt, rotational axes misalignment and boresight error.

The levelling of the heliostats was done from the bottom up, eliminating each preceding error. The first step was to compensate for the global tilt of the pod by simply adding spacers under two of the three pod feet. The individual pedestal tilt

was eliminated by replacing the six flange bolts with three longer bolts that separates the two flanges with nuts on both sides. This arrangement allows the plane of the slewing drive to be very accurately levelled, illustrated in Figure 24 below.

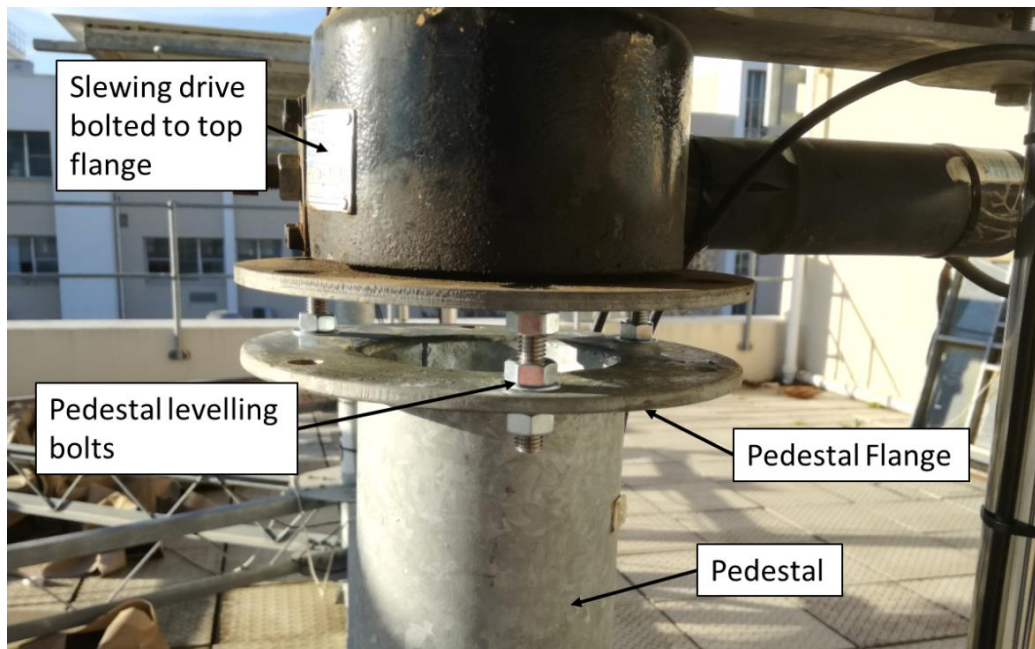


Figure 24: Eliminating the pedestal tilt

A tubular spirit level and digital inclinometer was used to eliminate the tilt error during the levelling process. The pedestal tilt was reduced to less than 0.2 degrees, as it is the smallest error the digital inclinometer can detect. However, final adjustments were made with the spirit level, as it was found to be more accurate at predicting true level.

The final step was to align the axes and eliminate boresight error, both these errors were corrected by loosening bolts, moving the mirror facet and bearing assembly relative to each other and tightening the bolts while keeping the parts aligned using the tubular spirit level. Table 3 below lists the averaged misalignments measured before and after the alignment for the 6 pod mounted heliostats.

Table 3: Average measured misalignment errors before and after levelling

Error source	Maximum Error measured on pod heliostats	
	Before Alignment	After Alignment
Pedestal tilt	2.1 °	< 0.2 °
Boresight error	1.8 °	< 0.2 °
Rotational axes misalignment	1.3 °	< 0.2 °

5 Helio­stat controller development and testing

This chapter presents the development of the helio­stat controller, from the first prototype to the final version.

5.1 First prototype helio­stat controller

After the basic principles of helio­stat control were researched, the first logical step was to design and build a controller and get a simple helio­stat control program working. The hardware and control program could then act as the foundation to which further functionality and complexity could be added.

5.1.1 Prototype 1 hardware breakdown

As mentioned, the helio­stats incorporate the azimuth and altitude design configuration, with both actuators requiring 24 volts DC. The electrical cables connecting the actuators to the controllers have two motor input wires, two encoder power inputs and two encoder signal outputs. As these actuators are the only two components that have to connect to the controller, they set the requirement for the input output structure of the helio­stat controller.

The first prototype controller was put together using an Arduino Uno microcontroller with & SD card reader, a dual H-bridge DC motor controller, a DC-DC stepdown (Buck) converter, an analogue two axis joystick and an optical isolated encoder signal conditioner as shown on Figure 25.

All the hardware components of the controller mentioned are inexpensive, all of which were off the shelf items, except for the encoder signal conditioner. Its purpose is to convert the 24-volt encoder square wave output signals to a microcontroller compatible five volts. At first a normal voltage divider circuit was built to generate the desired 5-volt output signal. However, electrical noise was present in this method of reducing the signal voltage, causing the microcontroller to read false encoder steps. The solution was to build a simple signal conditioning circuit (visible on Figure 25) incorporating opto-isolators. These are semiconductor devices that transfer an electrical signal via a short optical transmission path between two elements of a circuit, while keeping them electrically isolated from each other.

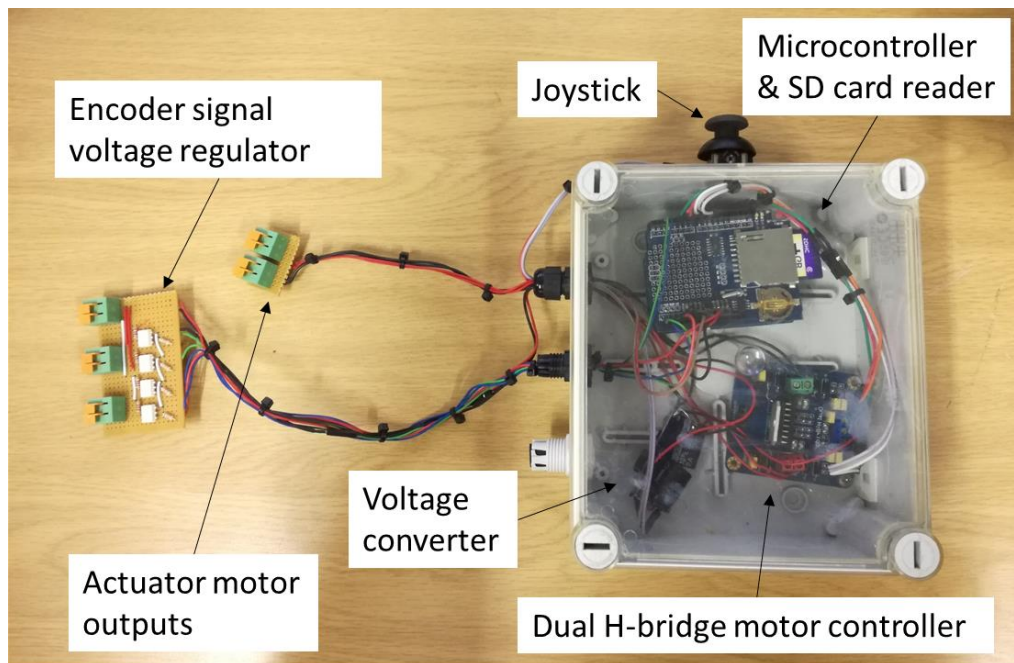


Figure 25: First prototype heliostat controller

A lot of experience was gained constructing the prototype controller, especially the art of electrical problem-solving.

5.1.2 Heliostat control program version 1

As soon as the controller was assembled and working, the first version of the heliostat control program was created and tested. This section will explain the functionality and structure of the first version heliostat control program, as well as its performance and ease of use.

Functionality

To start the tracking of a heliostat, all the actuator wires are first connected to the controller via the electrical wire clamps. (These clamps allow the controller to be portable and easily connected to any heliostat for testing purposes.)

After switching on the controller, the operator uses the joystick mounted on the side of the controller's enclosure to manually move the sunspot to the middle of the receiver (i.e. the tracked position). This task is intuitive, and it is recommended that the operator starts with the sunspot reflecting onto the ground and proceed to move the sunspot up the tower and onto the receiver. Once the sunspot is in the tracked position, the operator enters the current time to the nearest minute into the Arduino integrated development environment (IDE) serial monitor via a laptop, which is sent to the microcontroller via a USB connection. Thus, the only input needed to finish the calibration and start tracking is the manual joystick movements to focus the heliostat's sunspot onto the receiver and the input of the current time. Once the heliostat is tracking, it can be disconnected from the laptop. During a test the heliostat can also be re calibrated by resetting the microcontroller and repeating the steps above. A flow diagram of the program

overview is shown on Figure 26. A more detailed flow diagram of only the heliostat tracking function is shown on Figure 27

The joystick's analogue output voltage signals were mapped to a pulse width modulated (PWM) duty cycle to control the speed of the actuators. This made accurate control of the sunspot position possible, resulting in a fast and easy calibration process.

Program Structure

The program only has a calibration and tracking function, resembling the simplest form of an open loop heliostat control program, with feedback of the heliostats position obtained from the actuator's internal rotary encoders. Figure 26 below shows the program flow diagram.

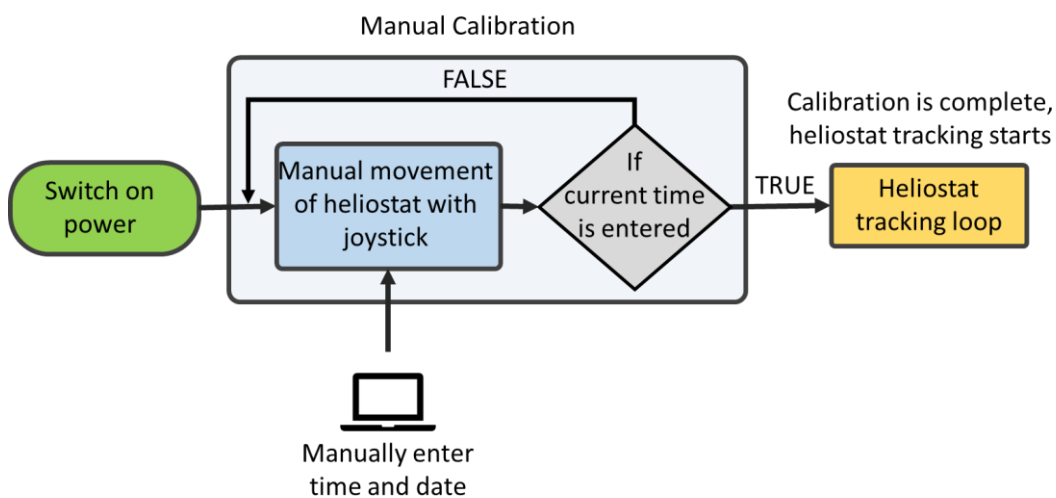


Figure 26: Flow diagram of the first heliostat control program

Calibration

When the heliostat is positioned by the operator to reflect onto the aiming point, the heliostat is in the tracked position. Thus, the assumption that the heliostat's altitude and azimuth angles are equal to the tracked altitude and azimuth angles for that specific time must be true, which forms the logic the calibration process is based on. The moment the operator enters the current time, the microcontroller retrieves the corresponding solar angles from the SD card, calculates the tracked altitude and azimuth angles using equations 2.2 and 2.3 mentioned earlier, and sets them equal to the heliostat's current altitude and azimuth angles. The calibration does therefore not rely on microswitches to establish a home or reference position.

The reason for the simplicity of the calibration process is due to the assumption that no misalignment or other tracking error sources are present. Furthermore, the position of the heliostat relative to the receiver and the facility's geographical location remains constant. This leaves the solar position as the only variable changing over time.

As mentioned, the solar positions used by the microcontroller for the tracking calculations are stored on a SD card. This was done to further simplify the controller programming, by doing away with the calculation of the solar angles during a test. Thus, a once off calculation of a whole year’s effective daylight solar positions with 30 second increments was completed using the NREL (SPA) and Matlab. The SD card reader is visible on Figure 25.

Tracking

The tracking function computes the bisection vector (heliostat pointing vector) every time the update interval is reached, calculates the required encoder steps to reach the new bisection vector (tracked position) and powers the actuators until the new tracked position is reached. Figure 27 below shows the tracking function flow diagram.

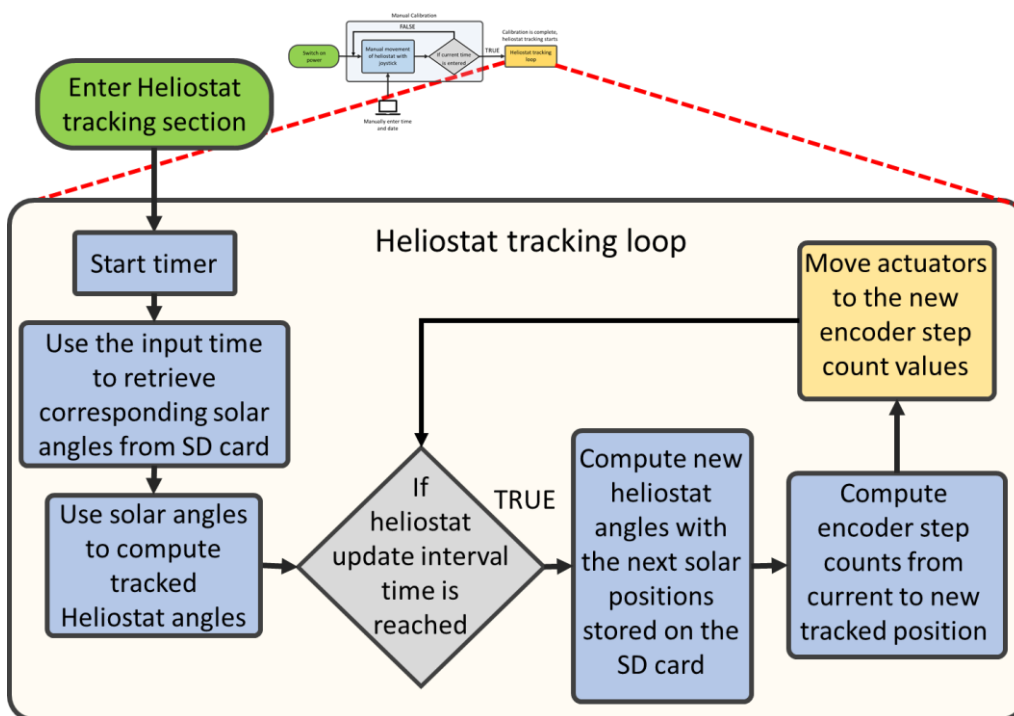


Figure 27: Heliostat tracking loop

The actuator control function that switches on the actuators while constantly comparing the current encoder values to the encoder setpoint values for each position update was perfected during these tests and formed the basis for all the future functions that required a position update. The flow diagram of the actuator control function is shown on Figure 28.

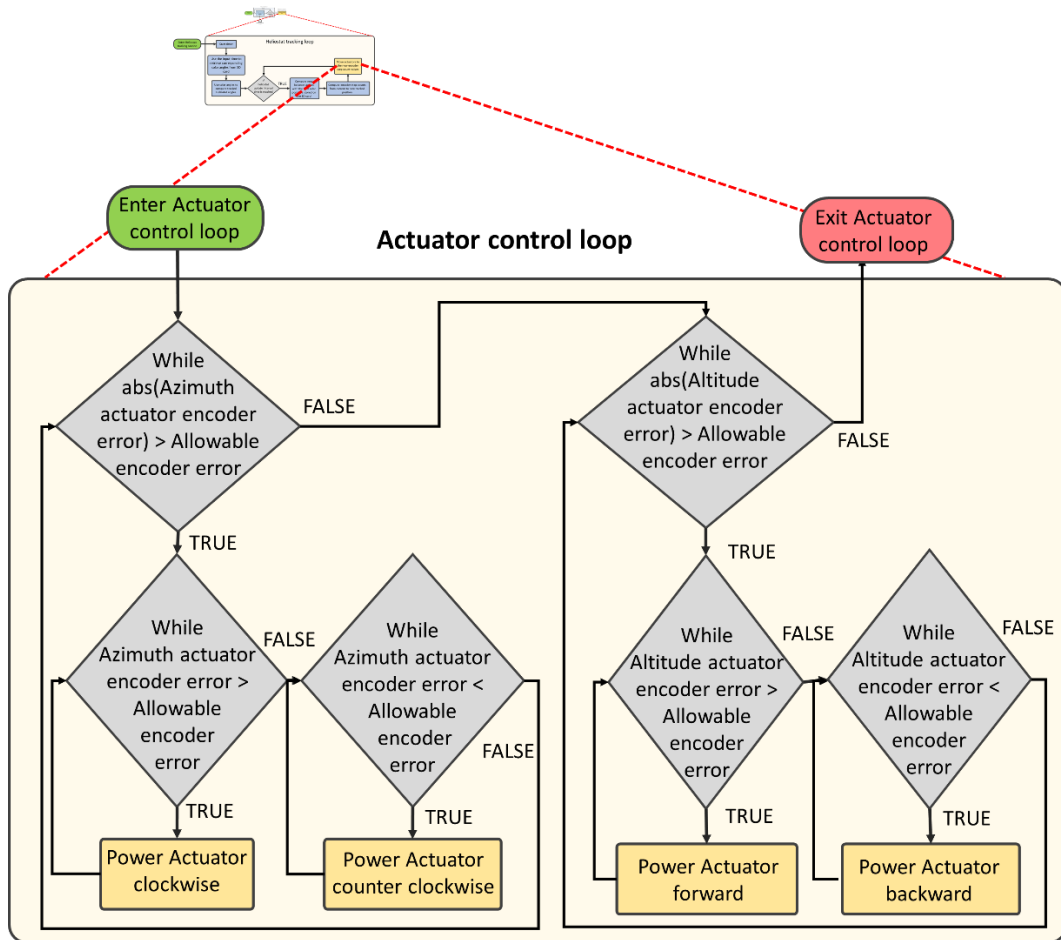


Figure 28: Actuator control loop

5.1.3 Tracking performance

The prototype controller performed as intended with no failures or shortcomings noticed. The precise manual control the joystick gave the operator over a heliostat was found to be a feature with potential for application in future versions of the calibration function. Furthermore, multiple tracking tests spanning 1 – 3 hours were carried out and documented with time-lapse photography. Figure 29 shows three screenshots that were captured from a time-lapse video of a tracking test which spanned two hours.

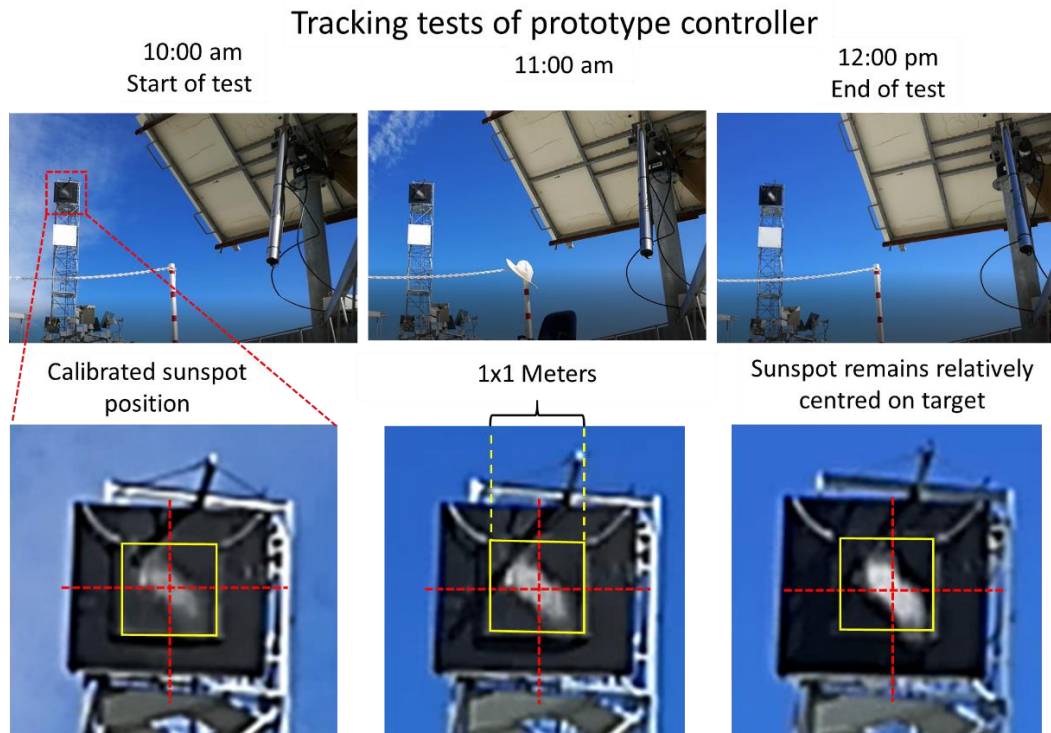


Figure 29: Tracking response of a 2-hour tracking tests of the prototype controller.

The individual screenshots of Figure 29 show the tower in the background and the back of heliostat number one on the right. If the three images are compared, the shift in heliostat facet position is clearly visible, especially when looking at the position of the linear actuator. The sunspot is clearly visible on the black receiver target, and its estimated centroid is marked with a red cross. The yellow square highlights the outline of a 1x1 meter corrugated steel target that was fixed to the front of the tower (this target was later removed and replaced with an experimental receiver). The time-lapse video of the two-hour test validates that the tracking program was functioning correctly, and also implies that the assumptions made regarding the heliostat alignment were not unrealistic. The final screenshot was analysed, and it was determined that the centroid of the sunspot drifted approximately 0.07 m to the right and 0.10 m downwards. This drift error is acceptable if the application of the facility is considered, where it will be used for experimental receiver tests utilizing the peak solar insolation window around solar noon. The implementation of an error model was considered, however the tracking accuracy the tests produced is satisfactory, and the remaining time would be more productively spent developing and testing more tracking functions as well as an intuitive user interface to make the facility easy to use for newcomers.

5.2 Second prototype heliostat controller

With the first prototype heliostat controller working, the next step was to add more functions, and a graphical user interface from which the heliostats can be wirelessly controlled.

5.2.1 Prototype 2 hardware breakdown

The only difference regarding the hardware of the second prototype, is the microcontroller and the removal of the joystick.

The new microcontroller selected for the second prototype controller was the NodeMCU, incorporating the ESP8266 microchip. The ESP8266 is a very low cost, 32-bit, Wi-Fi enabled microchip with a clock speed of 80 MHz. The microcontroller was chosen mainly because of its Wi-Fi capability, however its low cost, Arduino IDE compatibility and the amount of documentation and support available online was also a large deciding factor.

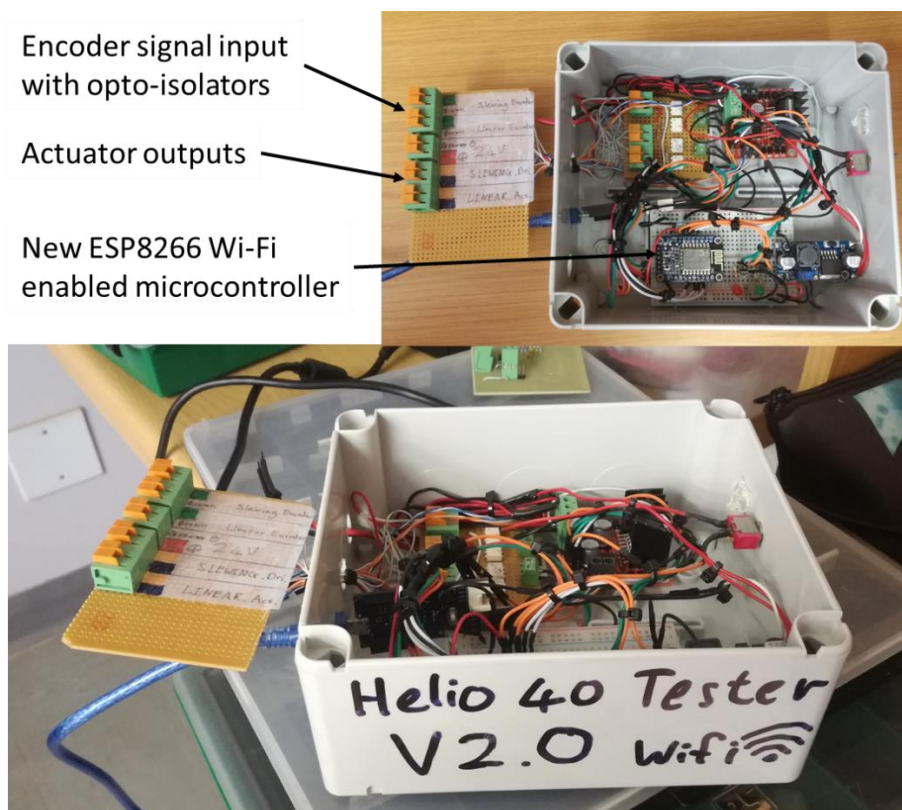


Figure 30: Second prototype Wi-Fi enabled heliostat controller

The removal of the joystick was a result of the creation of a user interface that is accessed from a PC, smartphone or tablet which interface with either a touchscreen or a keyboard and computer mouse. The joystick could still be incorporated into the control system, however it will act as an intermediate interface device requiring its own microcontroller and control hierarchy in the programming, adding to the complexity of the system. For this reason, a similar method of manually controlling the heliostats was developed using the device's existing interface. The method is further discussed in section 8.3.3.

5.2.2 Prototype 2 Wi-Fi communication

With the Wi-Fi communication capability of the microcontroller, data can be wirelessly transmitted between the heliostat controller and any another connected device. This communication requires a Wi-Fi access point for the heliostat controller, and a user interface that can be accessed by the device one wishes to control the heliostat from.

From the start it was decided that the heliostats should connect to the internet and not a local network. The reason therefor is the added flexibility in terms of the device and location you wish to control the heliostats from. For example, if the user interface is web-based, the heliostat operator can control the heliostats from his smartphone or tablet using a mobile connection, while standing amongst the heliostats out of the confinement of the control room where only the pod heliostats are in sight. Another advantage of the web-based approach that is especially important for the Helio40 facility, is the fact that the accessibility of the user interface is not dependent on a specific PC, installed software, operating system or the reliability of a local network. This adds a level of robustness to the control of the facility that is well suited for a research environment that is continuously evolving. Figure 31 below shows the basic connectivity architecture of the Wi-Fi connected heliostats.

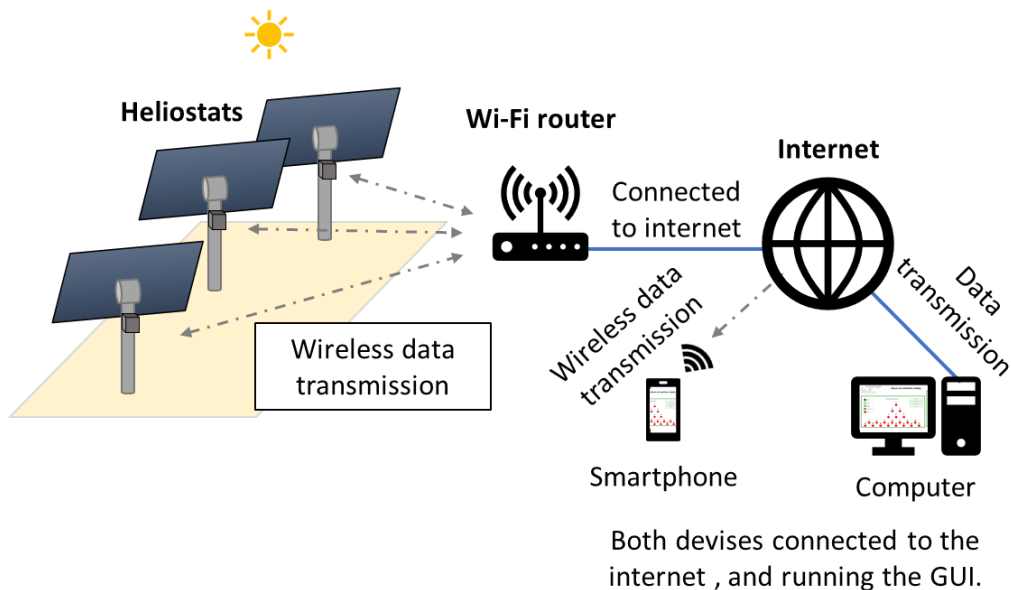


Figure 31: Wi-Fi communication architecture

A practical benefit of connecting the heliostats directly to the internet using Wi-Fi, is that all the needed communication infrastructure already exists in the control room in form of Ethernet access ports. As a result, no data cables are needed between the heliostats and the device running the web-based control interface. The only communication hardware that was added to the system was a Wi-Fi router dedicated to the heliostats, serving as the internet access point.

During the initial tests of the Wi-Fi enabled heliostat controller (before the dedicated Wi-Fi router was installed as the internet access point), the author's smartphone was used as a Wi-Fi hotspot while also running the user interface. This was only a temporary solution that was used to test the early versions of the program while waiting for the router to be installed. During these early tests it was found that being right next to the heliostat made debugging very convenient, as the movement (output) of the heliostat could be directly observed while entering control commands on the smartphone.

(Gross, et al., 2017) developed a universal heliostat control system, designed for commercial size CRS plants. The control system architecture described by Gross is similar to this project with regard to the GUI being independent of a specific machine. The authors state that this method supports multi-operator access that was exploited with the implementation of a suitable hierarchy of user rights. For this project however, all users who access the GUI will have full access to all the functions. This implicates that for example the receiver operator/researcher can adjust the receiver flux requirements or completely defocus the field if necessary, while the heliostat field operator is outside keeping an eye on the heliostats, while the GUI is open on his smartphone or tablet. This is yet another beneficial feature of the web-based approach.

5.3 Final heliostat controller design (PCB)

After the experience gained from designing constructing and testing the prototype controllers, a final circuit had to be designed for permanent installation at the facility.

Final heliostat controller hardware

The ESP8266 microchip performed well, as expected, except for the NodeMCU development board it was attached to. The microcontroller had connection issues and suffered from intermittent errors when trying to upload programs. At first it was thought that the connection issues were due to a faulty Wi-Fi router, however, after testing the connection strength with a smartphone from various positions from the router, it was established that the small Wi-Fi antenna on the NodeMCU PCB was the culprit. As a result, the Sparkfun Thing Development Board (also incorporating the ESP8266) was chosen as the replacement microcontroller.

The L298 dual H bridge motor driver incorporated into the prototype controllers was also replaced. During the prototype testing, a few L298 drivers burnt out. This was found to be a result the of the high starting currents of the DC motors powering the actuators. The problem was mitigated with a soft start function that was added to the motor control programming. Although effective in reducing the starting current spikes, drivers were still occasionally burning out, suggesting that the 2 Amp maximum current rating of the motor driver was not sufficient. The new motor driver that was selected is a dual H bridge 6 Amp 30V DC motor driver from hobbytronics.co.uk. The signal conditioning circuit that was built for the first prototype controller performed without any problems and was consequently integrated into the final controlled design.

The electrical connections between the hardware components were completed using a breadboard and various soldered wires in the prototype controllers. For the final version of the controller, it was decided to design and manufacture a printed circuit board (PCB) to connect all the components. Before the PCB was designed, a final prototype controller was built, this time on perforated prototyping board with the intention of finalising the orientation and spacing of the components, as well as ensuring that all the electrical connections were correct. The design of the PCB was completed using the free online software from easyeda.com. The website also offers a direct online PCB ordering service by JLCpcb, a Chinese company that is famous for manufacturing and delivering cheap high-quality PCB's anywhere in the world in less than a week from submitting the Gerber files. Figure 32 shows the top view of the bare- and populated PCB.

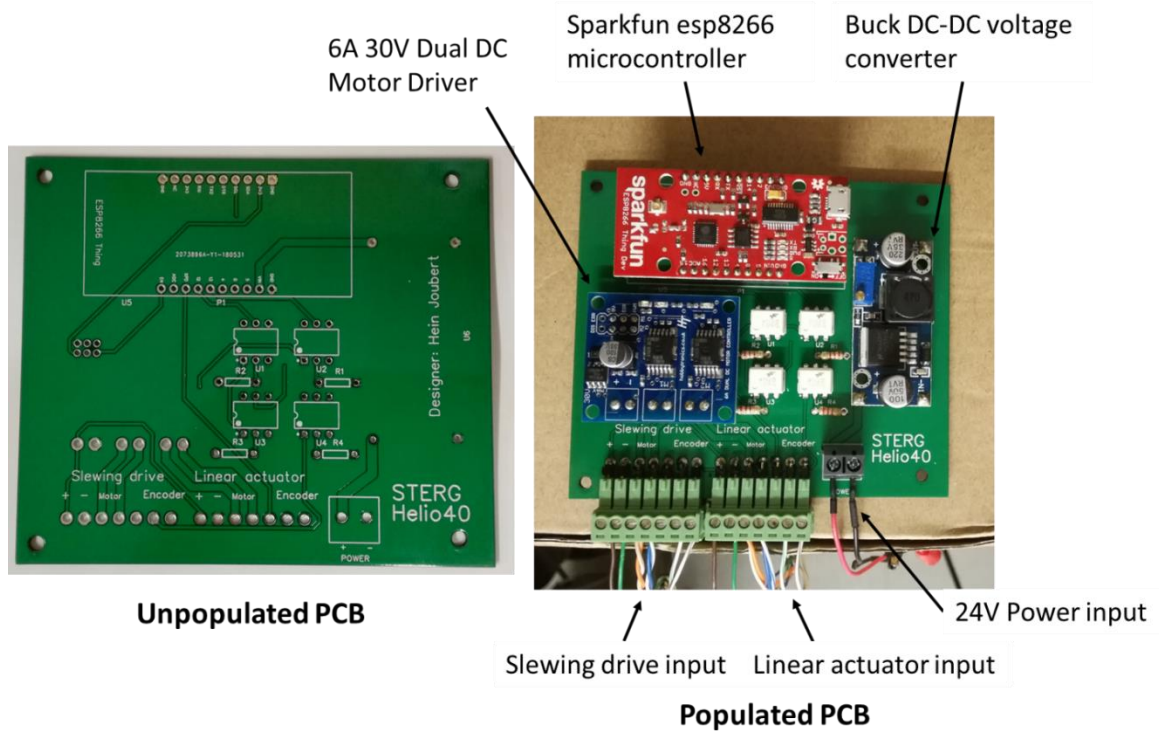


Figure 32: Final Helio40 controller

The design of the final controller incorporates 2 plug connectors for the separate actuators, and a screw terminal connector for the 24-volt DC power input. The actuator plug connectors eliminates the possibility of connecting the 6 wires between each actuator and the control board incorrectly. This was an issue identified on the original Helio40 control boards. The microcontroller is connected to the PCB with standard pin header connectors, which can be easily unplugged. This makes it convenient if a new version of the heliostat control program needs to be uploaded to the microcontroller, or in case of component failure.

6 Helio40 graphical user interface (GUI)

Up to this point the communication between a heliostat and the operator had been through the Arduino IDE command-line interface, that requires specific commands to be typed on a computer keyboard. In this chapter the GUI that serves as a control panel for the facility is presented.

A well-designed GUI enables the operator to accomplish the goal through an interaction that is as simple and efficient as possible. The interface should therefore only display information that is relevant to the task that needs to be completed and should also have a distinct logical layout where similar information and functionality are grouped together. Furthermore, the effectiveness of a GUI can be enhanced by making the interface aesthetically pleasing, without drawing unnecessary attention to itself.

For this research project, the GUI is key to ensure the safe and efficient operation of the system, as the facility will have new operators with not the same level of expertise as the author of the project.

6.1 Required functionality

Before work began on the user interface, the fundamental functionality of the system had to be specified to set up a starting point for the first version of the GUI.

For the heliostat field of CRS systems there are 4 main functions that are essential to their operation namely; calibration, tracking, defocus and stow. These were the four main functions incorporated into the first iteration of the control system. When these 4 functions are examined, it becomes clear that tracking and calibration are the two main functions and defocus & stow are based on the tracking function logic (just moving to new specified actuator positions). For example, the defocus function is essentially the tracking function with a different aimpoint. This aim point is usually chosen to be above the receiver tower in commercial CRS plants.

6.2 Outsourcing of GUI & web hosting

Upon researching the different options available to create a web-based GUI, it was quickly realised that standard HTML, CSS and JavaScript programming had to be used to create the control panel. The reason being, the unlimited amount of freedom regarding the layout and functionality of the control panel, compared to the alternative of using free application development websites. These free application development platforms were developed for simple projects such as home automation instead of complex control panels.

The creation of a website such as the one required is generally done by web developers following a technical specification. Since web development falls outside the scope of this project, the decision was made to outsource the creation and hosting of the GUI, similar to a mechanical part that requires engineering

drawings to be manufactured by a machinist. The technical specification included a visual mock-up of the control panel (GUI) also known as the “front end”, and the relationship between the buttons and the variables in the data tables forming the rear-end.

Endeman, a company based on the outskirts of Cape Town was approached for the outsourcing. The author worked together with the web developer to create the GUI, acquiring a lot of skills and learning new programming languages in the process. Once the goal of creating a simple GUI with the four main functions mentioned above was reached, the author continued to modify and improve the GUI without help from the company. The initial mock-up of the control panel is presented on Figure 33 below. The layout of the final GUI and its functionality is thoroughly explained in the following sections and chapter seven. The final GUI strongly resembles the original mock-up, although as testing of the facility proceeded, various changes were made, adding more functions and flexibility to the GUI.

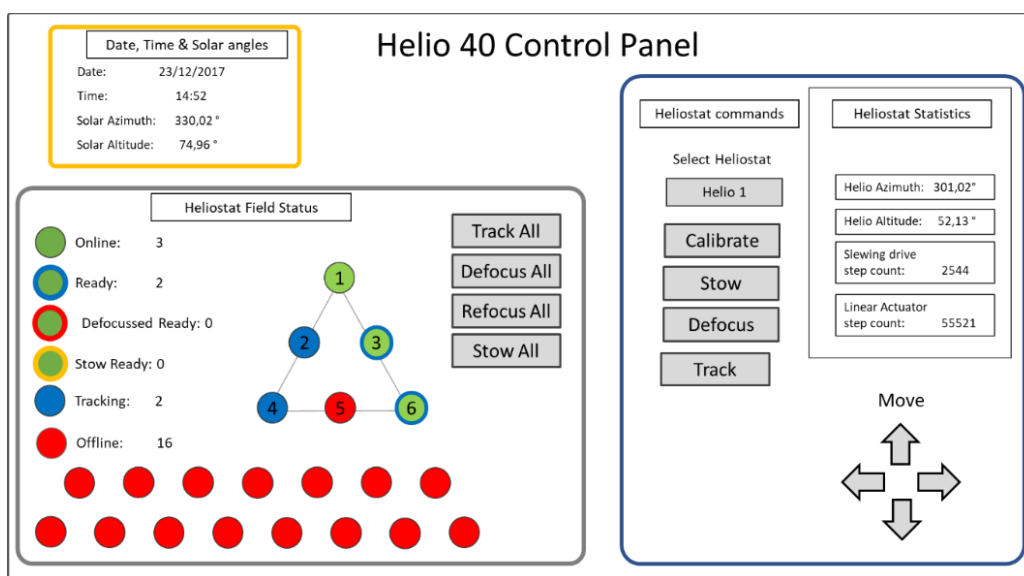


Figure 33: Mock-up of GUI

6.3 Helio 40 controller & GUI communication

With the current hardware configuration, there are two main approaches that can be followed regarding the location where the main heliostat control program is run. One of the methods would be to do the bulk of the calculations on the microcontroller, and only send high level commands to the heliostats, while they operate mainly independently. The other method would be to have a server or PC as the “brain” of the system and send low level commands to the heliostats while most of the computation is done on the PC/server. These two methods of control each have their advantages and disadvantages, however, the method mentioned first (send high level commands to the heliostats) was chosen due to its compatibility with the web-based approach.

The structure of the final heliostat control program that runs on the microcontroller is therefore similar to the original versions developed during the prototype stage. The solar positions that used to be stored on the SD card, are now stored in a SQL database together with all the other information sent between the controller and the GUI. This SQL database can therefore be thought of as a card that is constantly read by the heliostat controller and edited by the GUI as the operator inputs control commands. This “card” also has entries where the controller enters information specific to the heliostats. These heliostat specific variables such as its status and azimuth & altitude angles are read by the GUI and displayed, informing the operator about the status and position of the heliostat. Figure 34 below shows the overview of this communication structure.

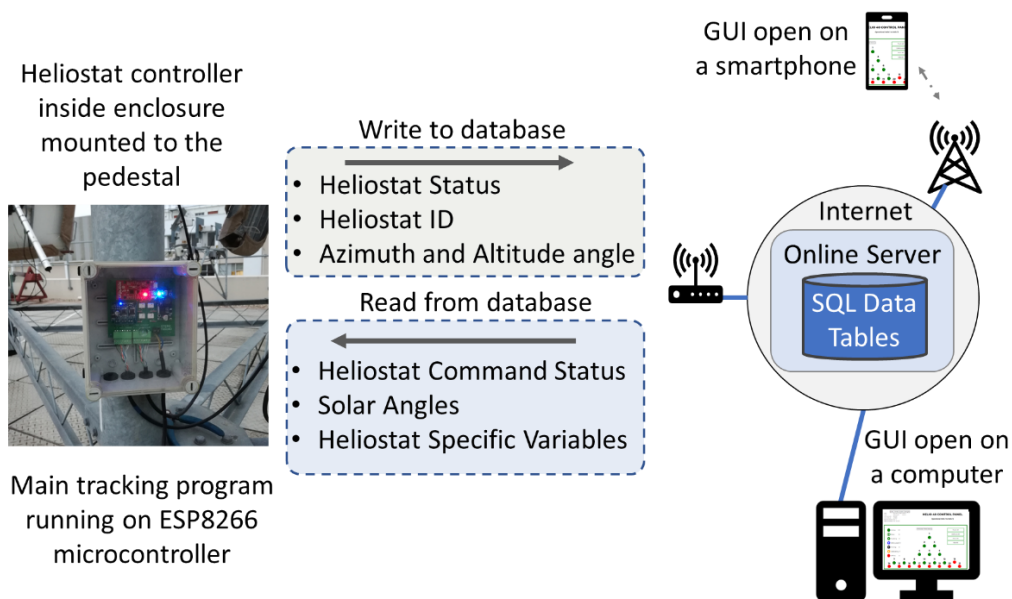


Figure 34: Communication structure between the heliostat controller, SQL database and the GUI

6.4 Graphical user interface (GUI) final version

In this section the final version of the GUI is presented. Its functionality is explored in the next chapter, by going through the steps that would normally be followed during a receiver test. A screenshot of the GUI is presented on Figure 35.

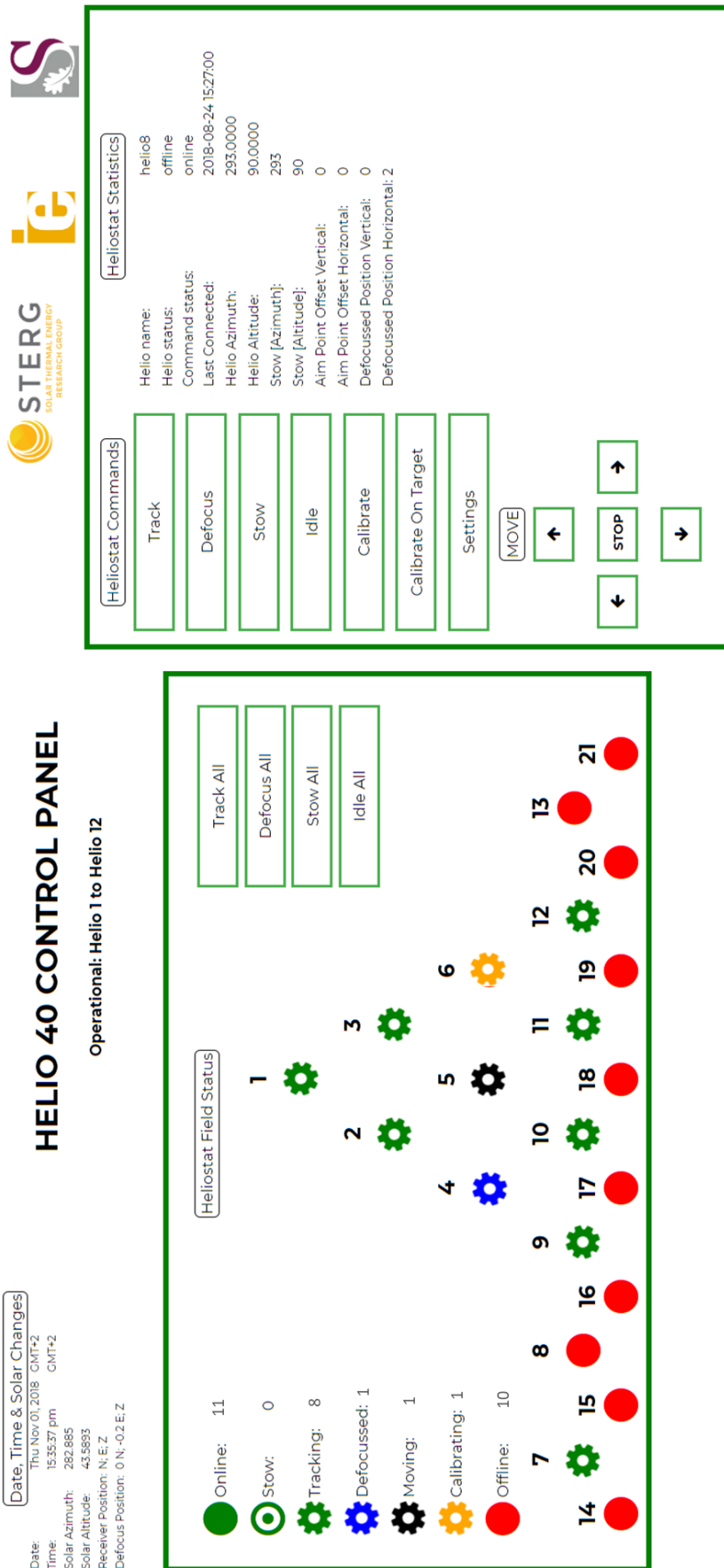


Figure 35: Final version of the Helio40 facility Graphical user interface

GUI breakdown

On the top left of the control panel, general information such as the current date, time and solar position of the facility is displayed. The functional section of the GUI is split into two main squares explained below.

Heliostat field

The left square shows the top view of the facility's heliostat field layout, where each heliostat is represented with a status icon and its corresponding ID number. On the left side of the left square, there is a heliostat status icon column, that shows all the different statuses a heliostat can possess, each with its corresponding shape and colour. The icons also have a number to their right, indicating how many heliostats currently have that corresponding status. It should also be noted that the heliostat status displayed on the GUI is the status received from the heliostat (as discussed in section 6.3). This means that the command status might have changed (displayed on the right-hand side square of the GUI under "Heliostat Statistics"), but if the heliostat does not connect, receive its new command status and sends back the its acquired status, the status icon on the GUI will remain unchanged. The commands "track", "defocus", "stow", and "Idle" can be given to the entire field from this square. These commands are explained in the following chapter.

Selected heliostat

The square on the right is dedicated to the selected heliostat (To select a heliostat the operator simply clicks on the corresponding heliostat icon in the heliostat field status block) and is subdivided into a command section and a heliostat statistics section. In the command section, there are seven commands that can be given to the selected heliostat, while the statistics section lists relevant information about the heliostat.

Heliostat settings window

In the right box containing the heliostat commands, there is a button labelled settings. If it is clicked, the heliostat settings window opens. In this settings window, general tracking parameters are changed that are explained in the next chapter.

7 Functionality of the recommissioned facility

In this chapter, the functionality of the final version of the GUI and heliostat control program is explored by explaining the standard procedures an operator would follow when performing a tracking test.

7.1 Powering up the facility

At the start of a test, the GUI is opened first. All the heliostats will have a status of offline, signified by the red circles on the control panel, illustrated on a screenshot of the GUI on Figure 36 below (Their status is always offline after the system has been shut down for longer than 5 minutes).

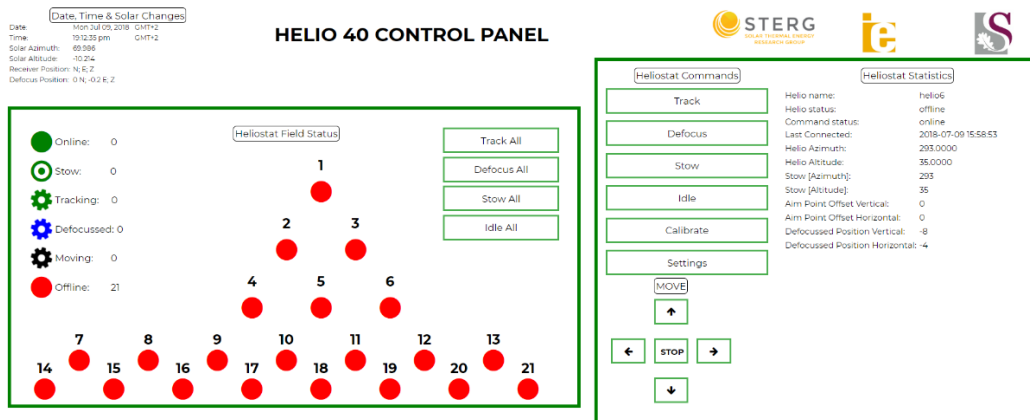


Figure 36: All heliostats offline, signified by the red circles

Next, the operator will visually inspect all the heliostats and confirm that their facet covers are installed, and their orientation corresponds with the altitude and azimuth angles listed under the heliostat statistics section in the GUI. This step is easily accomplished, as the heliostats should all be in the uniform stow position upon the start of a test. The facility can now be powered by switching on the system power switch located on the switchboard. The strobe warning beacons in the control room and the door siren in the opposite building will now be activated, signalling that the facility is in use.

The individual heliostats the operator wishes to use can now be powered from the heliostat switchboard. As the heliostats are switched on, they will connect to the Wi-Fi and their status will change to online on the control panel, signified by the green circles as illustrated on Figure 37. The online loop is essentially the idle condition for a heliostat, where it is powered, static and repeatedly connects, awaiting further commands from the GUI.



Figure 37: Control panel on the left showing heliostats connected to the Control panel, and the switch board indicating the heliostats are powered with the LEDs.

The lit LED's on the switchboard visible on Figure 37 shows that the heliostats are powered, this in fact does not mean that the heliostats are receiving power, as there is an intermediate power distribution box containing a relay and fuse in series (see section 4.1 for reference). Thus, if a heliostat is not connecting and showing up as online on the GUI, the operator should first make sure the heliostat is indeed receiving power at its control board.

7.2 Giving the first commands

Now that the field is online, four functions can be selected, namely track, defocus, calibrate or calibrate on target. As stated, the heliostats will most likely be in the stow position upon start up, and the general procedure is to command all the heliostats to defocus. This command can be given for the whole field simultaneously (defocus all), or each heliostat individually from the left side of the control panel. The controllers will retrieve the command status from the SQL data tables, enter the defocused loop, and send back the "moving" status to the control panel. The status icons will change to the black rotating gear, indicating that the heliostats are busy moving. The command status under the heliostat statistics will show "defocused", and the status icons will only change to the defocused blue rotating gear once the heliostat has successfully reached the defocused position. Figure 38 illustrates the change of icons on the control panel.

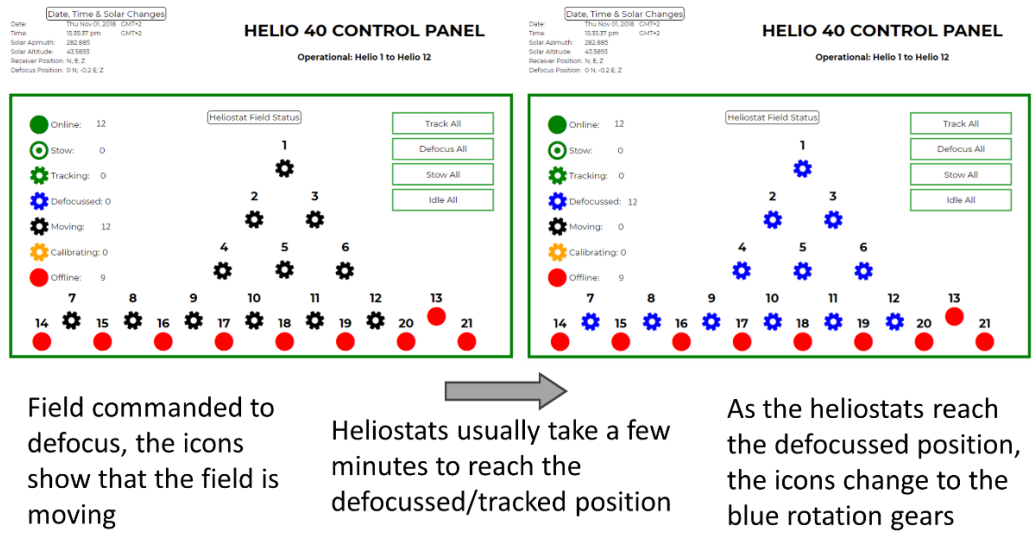


Figure 38: Heliostat field reaches defocused position

The heliostat controllers were programmed to send back the “moving” status if a heliostat has to move by more than 2 degrees, which is considered a “big” move in the control program. This 2-degree limit ensures that the icons do not constantly alternate between moving and defocused/tracked during the small periodic tracking updates that keep the reflected solar beam pointing at the defocused position in space.

When the whole field is in the defocused position, all the solar beams intersect at a point in space away from the receiver. This point in space (defocused position) can be changed by clicking on the “settings” button on the control panel and changing the vertical and horizontal distances relative to the receiver aimpoint. Thus, the defocused position is constrained to the plane intersecting the receiver aperture as illustrated on Figure 39.

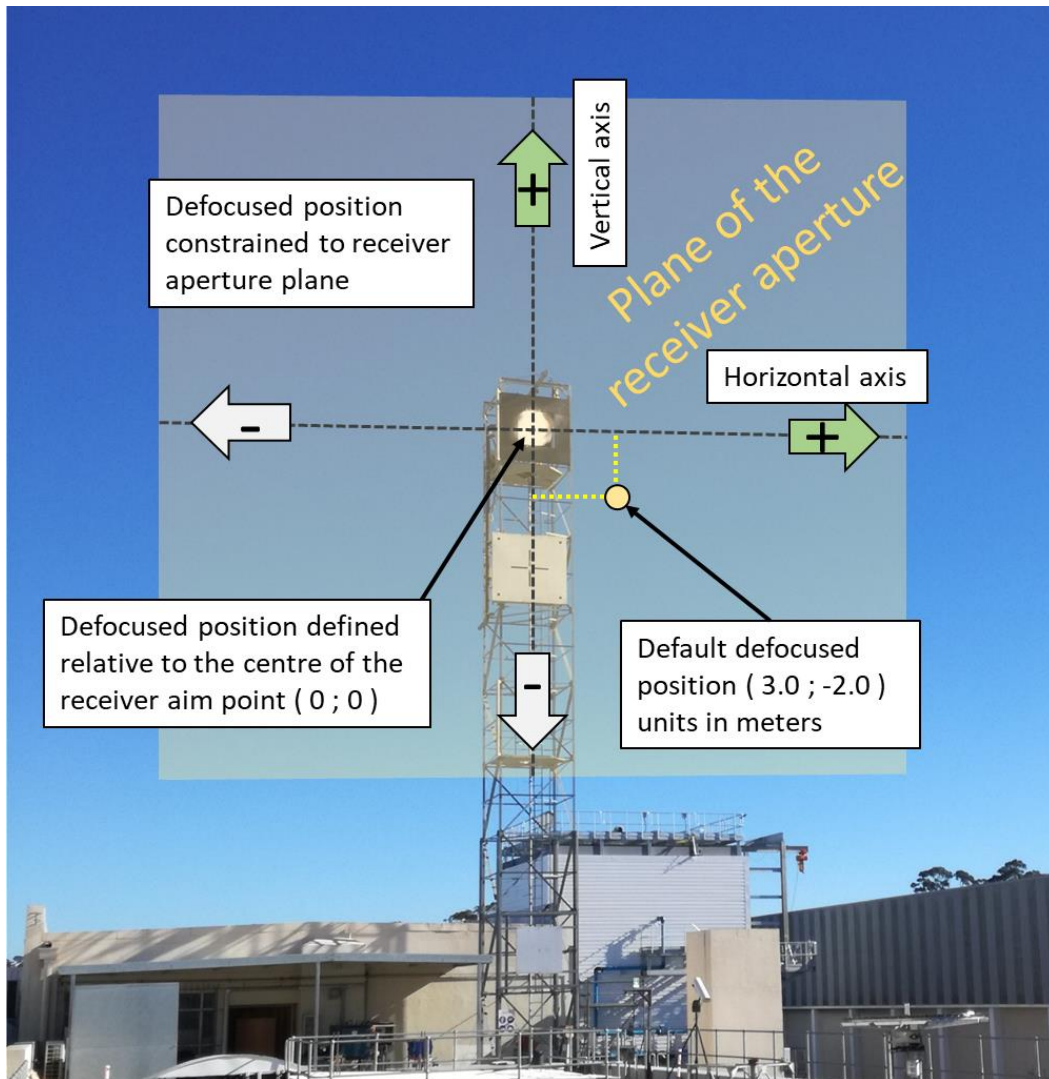


Figure 39: Defining the defocussed position

7.3 Calibration

The field is now ready to be manually calibrated which is essential for accurate tracking and should be performed for each heliostat before doing receiver testing. The control panel facilitates two methods of manual calibration, referred to on the control panel as “calibration” and “calibration on target”.

7.3.1 Calibration on target

The calibration on target command is advised to be used, as this method automatically moves the heliostat to the middle of the calibration target mounted below the receiver, using its position reference from when it was previously calibrated. When this command is selected, and the heliostat has completed the moving to the target, the icon on the control panel will change to the orange rotating gear, indicating that the heliostat is in the calibration loop. At this point the sunspot of the heliostat will fall somewhere on the target. Extensive use of the facility revealed that the error is typically in the range of 0.3 meters in either the vertical or horizontal direction.

The operator now manually eliminates this error by moving the sunspot to the centre of the target marked with a crosshair. These vertical and horizontal adjustments are made by moving horizontal and vertical sliders on the popup window that opens when the “calibrate on target” command is selected. The slider method was implemented due to its simplicity and compatibility with the keyboard & mouse and touchscreen interfaces. It replaced the joystick method described earlier. Figure 40 shows the calibration popup window with the sliders and a reference image illustrating a calibrated sunspot.

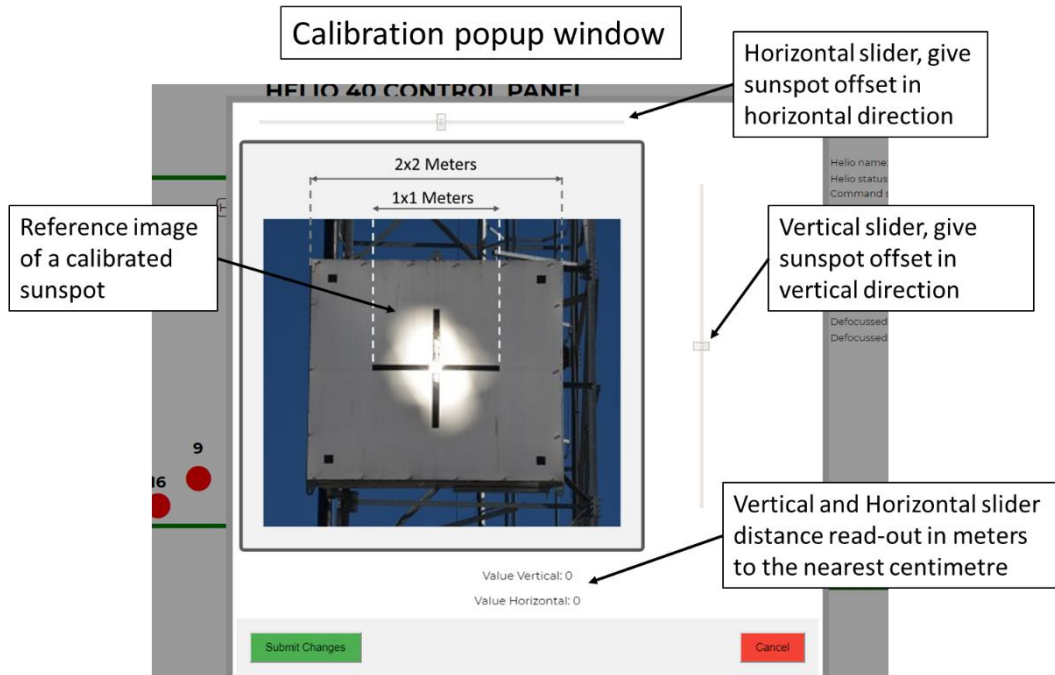


Figure 40: Calibration popup window

As soon as the operator has moved the sunspot to the middle of the target as illustrated on the reference image of the popup window, the heliostat is selected to defocus, completing the calibration procedure for the corresponding heliostat. After the operator has cycled through all the heliostats (which took the author just under one minute per heliostat), and they are all in the defocussed position, the command can be given for the whole field to track. All the sunspots will then move together to the receiver aimpoint, where they will continuously track, concentrating the solar radiation. Figure 41, shows the view of the tower and pod mounted heliostats from inside the control room, as well as a close up of the tower illustrating the calibration procedure. In Appendix A, 12 photos are shown of each individual heliostat’s sunspot calibrated on the receiver target, as well as an image showing the superimposed image of the 12 sunspots.

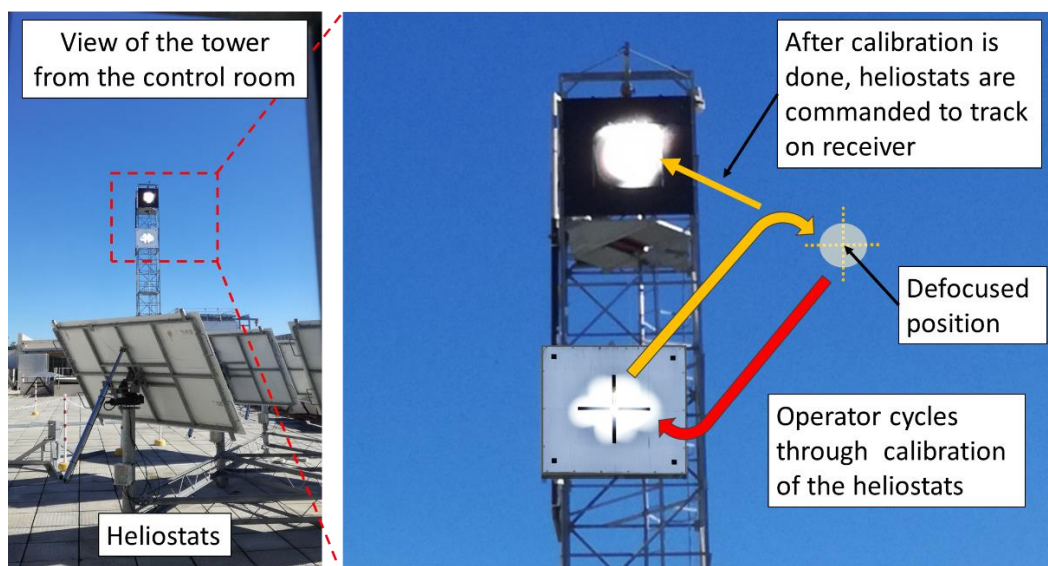


Figure 41: Illustration of the calibration procedure from the perspective of the control room

7.3.2 Calibration on receiver

The control system also facilitates another offset correction calibration function, which is a leftover from an earlier version of the control program. This function labelled “calibrate” on the control panel, is essentially the same calibration function that was used by the first prototype controller.

The operator uses the arrow keys on a keyboard or the arrow buttons on the control panel to move the sunspot of the heliostat to the centre of the receiver and select “track” to finish the calibration. If this calibration function is selected, the heliostat does not automatically move to the receiver aim point like the calibration on target function, and a heliostat should be selected to track first before choosing this calibration function. This method of calibration is not recommended, however it was kept a part of the control system, as this function gives the operator full control to move the heliostat to any required position (A feature that could be useful for future research purposes).

The speed at which the actuators move when this method is selected can be changed. With the speed of the heliostat reduced to 20 %, very precise manipulation of the sunspot is possible.

7.4 Tracking and tracking adjustments

Now that the heliostats are tracking on the receiver, the aimpoint can be changed for the whole field or a single heliostat in the settings window. This function was added to accommodate a receiver that is mounted off centre relative to the default tracking aimpoint show in Figure 42. Moreover, it can also function as a quick fix calibration offset, to correct tracking errors (although a target calibration is recommended). The aimpoint is changed by entering the desired aimpoint coordinate (horizontal & vertical) into the settings window (identical to the defocused position adjustments). The coordinate entered into the settings

window must be in meters and is defined relative to the default tracking aimpoint with coordinates (0;0). Figure 42 shows the process of changing the tracking aimpoint in the heliostat settings window.

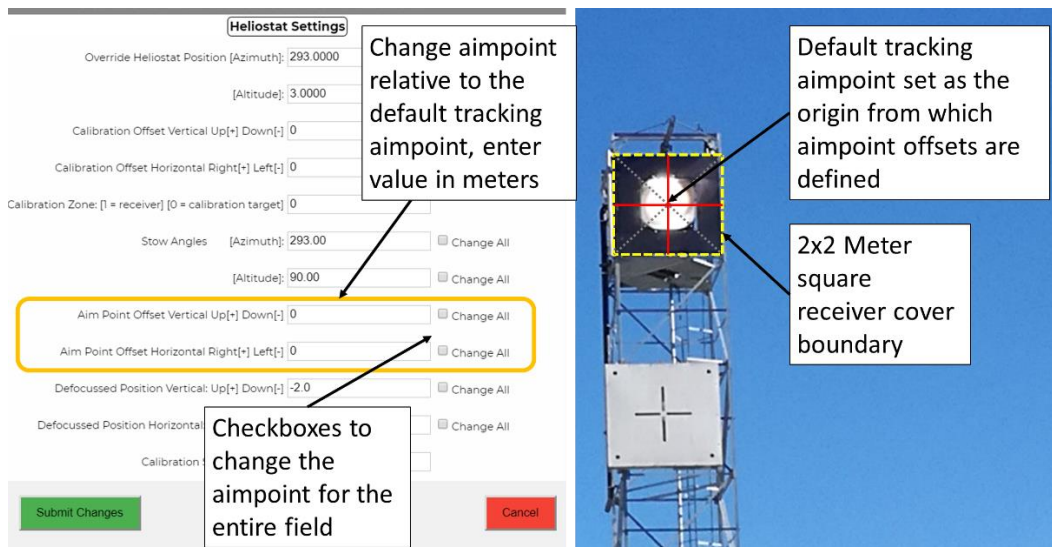


Figure 42: Tracking aimpoint adjustment

7.5 Stow and shutdown

When a test is complete, the facet covers are installed and the whole field is selected to stow. The only functionality of this function is to move the heliostats to the stow angles entered in the settings window (default stow angles should be 90 degrees altitude and 293 degrees azimuth). Each heliostat can be given its individual stow angles, thus the stow function can also be used to move each heliostat to any specified position within the actuator limits. Once all the heliostats have reached their stow positions as indicated on the control panel and confirmed with a quick visual inspection of the field, the facility can be powered off. Figure 43 summarizes the steps that were followed to conduct a test with a flow diagram.

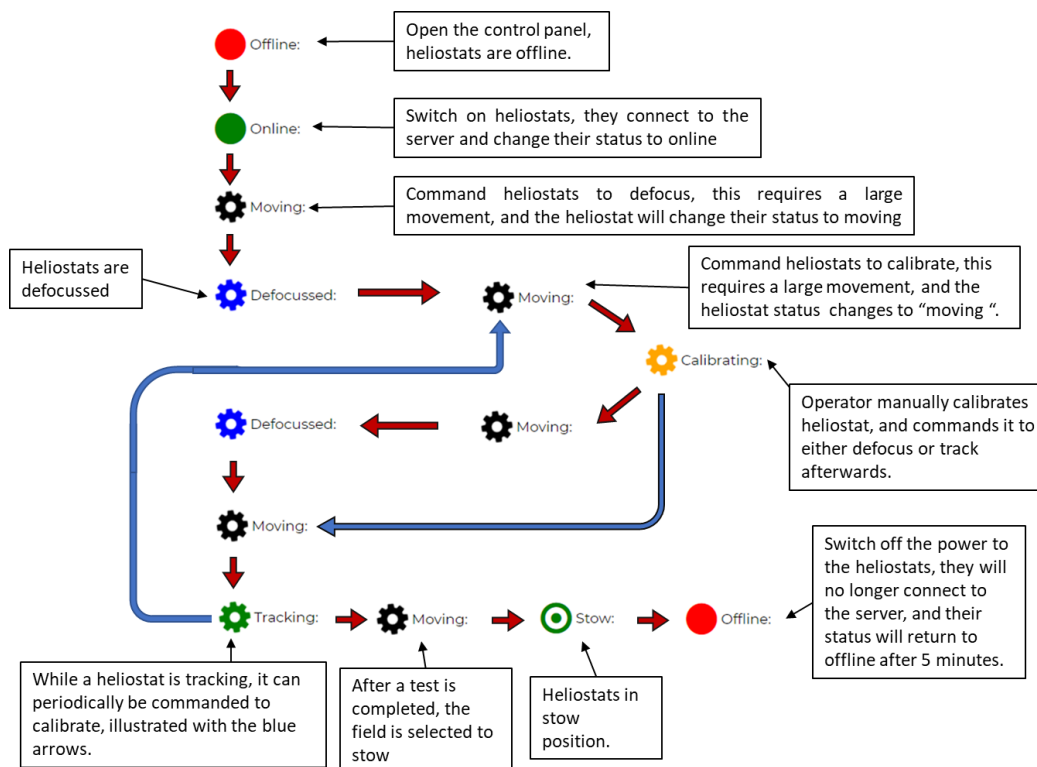


Figure 43: Typical Helio40 facility test, status flow diagram

7.6 Recovering a “lost” heliostat

It should be pointed out that a heliostat must not be switched off while it is moving, as the controllers do not communicate with the GUI during this period. The result of switching off a heliostat while it is moving is the loss of its position. A heliostat’s position is lost when the altitude and azimuth control system angles are completely different from the actual altitude and azimuth angles of the heliostat (indicative of a heliostat not reflecting on the target, when the “calibrate on target” function is selected). The 2 methods that can be followed to recapture the heliostat position is discussed in the following section.

Override heliostat position

A heliostat that lost its position can be manually calibrated by correcting the heliostat facet altitude and azimuth angles that are stored in the SQL database using the “override heliostat position” function. This requires the heliostat facet angles to be measured. Although the mirror altitude angle can be measured with an inclinometer, the azimuth angle is not easy to measure accurately. Thus, the recommended procedure is to move the heliostat to point forward, parallel with the solar roof as accurately as possible, and override the azimuth angle with the known heading of the roof (293 degrees).

An alternative to the altitude angle measurement using a digital inclinometer is to manually move the heliostat to 90 degrees altitude using a spirit level. The method described is rough calibration that should be followed by a solar target calibration. A “lost” heliostat can also be calibrated following the process

described in section 7.3.3, however this is sometimes time consuming or not possible if the sun is behind cloud cover.

8 System operation

The time between the first heliostat test with the prototype controller and final tracking tests involving the 12 recommissioned heliostats was 11 months. During this time, the rigorous testing of the control system revealed areas where more functionality would be beneficial to the safe and efficient operation of the facility. These changes were made, and control system underwent a gradual evolution to arrive at the final version explained in the previous chapter.

8.1 Utilization of the recommissioned Helio40 facility

Towards the end of this project, the recommissioned Helio40 facility was extensively used to supply concentrated solar radiation for an experimental receiver research project. These tests signified the first active receiver tests to be conducted using the Helio40 facility on STERG's high temperature laboratory located on the roof of the mechanical engineering building at Stellenbosch University.

These receiver tests were conducted over a period of 2 months and totalled 35 hours of recorded receiver temperature data. Keeping in mind all the start-up, calibration and stow procedures that take place before and after the heliostats are tracking on the receiver, the operational time of the facility during these tests was much greater than the recorded 35-hour tracking period. This receiver research project was started at the same time of this project, with the intention of making use of the recommissioned Helio40 facility. A photo of the operational facility is shown in Figure 44, where the 12 recommissioned heliostats are tracking, reflecting their solar beams on the experimental receiver.



Figure 44: Final tests being conducted with 12 tracking heliostats

8.2 Operational findings

During these tests, the gradual drift (and sometimes dispersion) of the focal point was visible. This was also confirmed by the steady decline of the temperatures measured inside the experimental receiver over long test periods when no action

was taken to correct the errors. Figure 45 shows two screenshots that were captured from a time-lapse of the receiver during a tracking test. In the figure, the first image shows the focal region at the start of the tracking test, followed by the screenshot taken one hour later. By comparing the two images, the marginal drift of the focal region downwards and to the right is visible. This drift error was at the time mitigated with a global aimpoint offset. The time varying errors associated with pure open loop control and an offset correction calibration method was thoroughly documented by Stone back in the early 1980's.

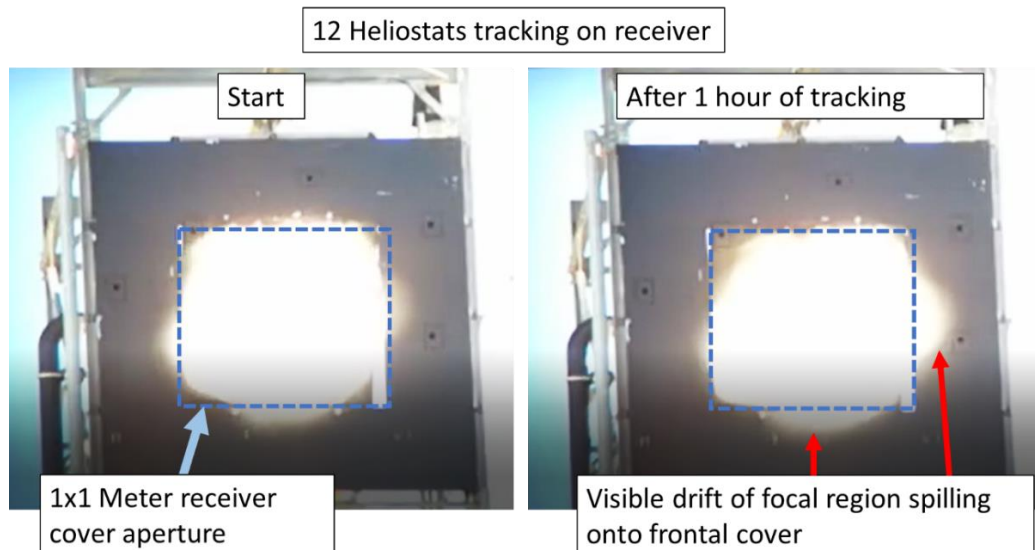


Figure 45: Observed tracking drift error

Although focal point drift can be eliminated using the aimpoint offset function relatively easily, focal point dispersion/expansion is more undesirable as it requires the suspect heliostats to be recalibrated. In order to recalibrate or adjust the aimpoint of the suspect heliostats, they first have to be identified. During the tests, this was done by wiggling the heliostats by hand while observing the focal point. This method of identifying heliostats in the high flux region of the receiver is in fact the manual version of the method described by (Bern, et al., 2017), which is discussed in the literature review.

The implementation of an error model into the control program would greatly reduce the time varying tracking errors present in the open loop tracking method as mentioned by (Malan, 2014). However, during lengthy tracking tests, it was found that the occasional recalibration and adjusting of aimpoints kept the facility operator busy and vigilant with attention focused on the field and GUI. The operator's attention should always be on the control panel and the heliostats due to the safety concerns mentioned earlier in the thesis.

After the receiver tests were completed, the burnt and discoloured paint on the steel plates surrounding the receiver cavity revealed interesting information. In Figure 46, the rusty red coloured oval shaped region around the 0.4 x 0.4-meter receiver cavity indicates where the heliostat beams were focused for the majority

of the 35 hours of testing. This discoloured region is well centred relative to the receiver cavity although it is slightly shifted to the right. The discoloration of the black paint occurred gradually, and it can therefore be compared to photographic film, where the discoloured zone is the “picture” developed by the exposure of the high solar flux region on the black steel plate.

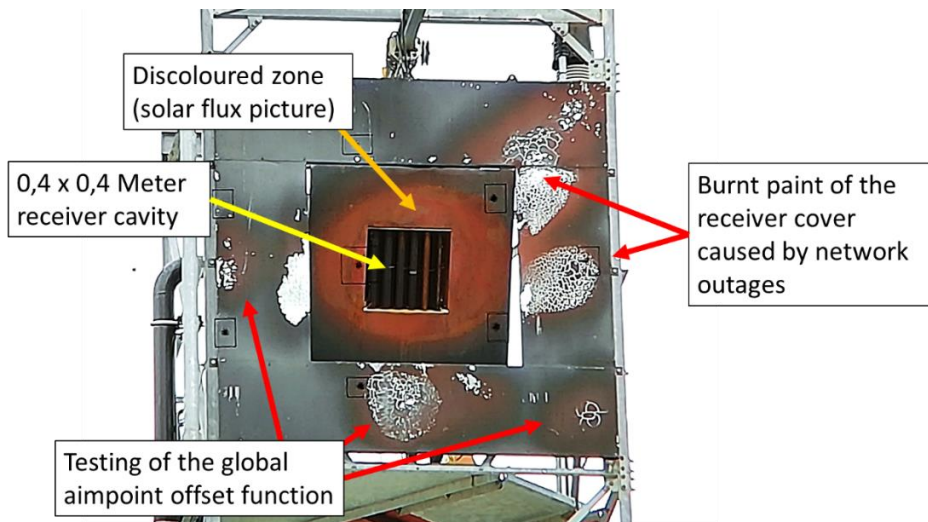


Figure 46: Experimental receiver after 35 hours of tracking tests were completed.

Also visible on the receiver outer cover are burn marks left over from aimpoint offset tests, as well as a burnt region to the right of the receiver that was caused by network outages. These network outages were caused by maintenance on the university’s network. At that stage, the function that automatically stows the heliostats after 5 minutes of not being able to connect to the GUI was not yet implemented (the incident led to the function’s implementation), and caused the sunspots to drift, leaving the burnt region in its path. The test during which the network outage occurred was recorded with time-lapse photography. Figure 47 shows a screenshot of the time-lapse that was taken during the incident.



Figure 47: Network outages prevented heliostats from updating their position, causing the heliostat beams to drift.

9 Conclusion

This project presented the recommissioning of a heliostat test facility and the development and implementation of a web-based control system that was tested and extensively used for receiver research. This chapter summarizes the work done, before conclusions are drawn and recommendations are made for future work.

9.1 Summary of work

Work which includes general mechanical maintenance, levelling of the heliostats, as well as the overhaul of the electrical wiring and safety systems was completed as part of the recommissioning process.

A heliostat controller was developed together with the heliostat control program. Three prototype controllers were built before the implementation of the final version heliostat controller. The heliostat control program underwent various iterations before arriving at the final implemented version. A simple calibration strategy was developed, specifically tailored for the Helio40 facility.

After the six pod mounted heliostats were recommissioned, there was enough time left and the six front row roof mounted heliostats were recommissioned as well. The GUI was developed implemented and rigorously tested during the utilization of the Helio40 facility for an experimental receiver research project.

9.2 Conclusions

The receiver tests that were made possible with the functional Helio40 facility, signified the first active receiver tests to be conducted on STERG's 18-meter receiver tower which forms part of the Helio40 facility.

The recommissioned facility functioned as intended and the GUI proved itself to offer the functionality required for the safe and efficient operation of the system. Furthermore, the use of colour and the logical layout of the control panel results in the interface being easily understood and minimizes the risk of confusion. The GUI can be opened on any device with an internet connection, making it possible for operators to control the facility from their smartphone while amongst the heliostats or temporarily out of the control room.

Safety measures were put in place to ensure the system is safe to operate in case of power or network outages. The safety features were experimentally demonstrated and came into effect during active receiver tests, circumventing possible emergency situations. The facility is currently operational and available for small scale CSP research with 12 heliostats currently recommissioned, having a total mirror area of 24 square meters. All the objectives of this thesis have therefore been successfully met and exceeded in some instances.

9.3 Recommendations for future work

9.3.1 Automated calibration offset

A feature that could easily be added to the control system, would be an automated camera calibration feature as described in the literature review by (Berenguel, et al., 2004).

The implementation of this feature will only require a camera, the image processing algorithm and an internet connection for the computer doing the image processing. The image processing can also be done on an online server, but then requires the image to be uploaded instead of only the two offset distances. Automated calibration will not significantly decrease the time the calibration takes, as most of the time of calibration is due to the heliostats moving to and from the defocussed/receiver position to the calibration target. However, one advantage of automated calibration is the ability to more accurately and repeatedly estimate the centre of flux intensity of the sunspot, as the current visual means of calibration is dependent on the operator's judgement.

9.3.2 Levelling of roof mounted heliostats

As the recommissioning of the roof mounted heliostats was not a main objective, they were not levelled. The levelling of these heliostats is recommended, as substantial misalignments can be observed while the heliostats are in the stow position.

9.3.3 Safety recommendations for use of facility

The fabric facet covers that cover the heliostats should only be removed when high temperature receiver tests are required. For all other tracking or control system tests, the facet covers should remain installed, using the small sighting holes in the covers to produce a sunspot on the intended target.

At the end of high temperature tests with uncovered heliostats, the covers should be installed while the heliostats are still tracking on the receiver to eliminate the risk of heliostats reflecting onto the neighbouring buildings while they are moving back to the stow position. The facility should always be supervised by two or more people while tests are carried out, to assist with the installation of the facet covers.

References

- Baheti, R. S., Scott, P. F. 1980. Design of Self-calibrating Controllers for Heliostats in a Solar Power Plant. *IEEE Transactions on Automatic Control*, Vol. AC-25.
- Berenguel, M., Rubio, F. R., Valverde, A., Lara, P. J., Arahall, M. R., Camacho, E. F., and Lopez, M., 2004. An artificial vision-based control system for automatic heliostat positioning offset correction in a central receiver solar power plant. *Solar Energy*, vol. 76, no. 5, pp. 563–575.
- Bern, G., Schöttl, P., Heimsath, A. & Nitz, P., 2017. Novel imaging closed loop control strategy for heliostats. *AIP Conference Proceedings*. 1850. 030005. 10.1063/1.4984348.
- Boese, F., Merkel, A., Stahl, D. & Stehle, H., 1981. A consideration of possible receiver designs for solar tower plants. *Solar Energy*, 11, 26(1), pp. 1-7.
- Convery, M. R., 2011. Closed-loop control for power tower heliostats. *SPIE Proceedings Vol. 8108: High and Low Concentrator Systems for Solar Electric Applications VI*.
- Curzon, F. L. & Ahlborn, B., 1975. Efficiency of a Carnot engine at maximum power output. *American Journal of Physics*, 1975;43:22–24.
- Dinter, F. & Möller, L., 2016. A review of Andasol 3 and perspective for parabolic trough CSP plants in South Africa. *AIP Conference Proceedings*, Volume 1734, pp. 0-10.
- Freeman, J., Kiranlal, E. U. & Rajasree, S. R., 2014. Study of the errors influencing heliostats for calibration and control system design. *International Conference on Recent Advances and Innovations in Engineering, ICRAIE 2014*.
- Gauché, P., Rudman, J., Mabaso, M., Landman, W. A., von Backstrom, T. W., Brent, A. C. System value and progress of CSP. *Solar Energy 2017*, Vol. 152, pp. 106-139.
- Goldberg, N., Kroyzer, G., Hayut, R., Schwarzbach, J., Eitan, A., and Pekarsky, S., 2015. Embedding a Visual Range Camera in a Solar Receiver, *Energy Procedia* 69, 1877–1884
- Gross, F., Geiger, M. & Buck, R., 2017. A Universal Heliostat Control System. *AIP Conference Proceedings*.
- Ho, C. K., Ghanbari, C. M. & Diver, R. B., 2011. Methodology to Assess Potential Glint and Glare Hazards From Concentrating Solar Power Plants: Analytical Models and Experimental Validation. *Journal of Solar Energy Engineering*. 133. 10.1115/ES2010-90053.

- IRENA, 2018. Renewable Power Generation Costs in 2017. IRENA - *International Renewable Energy Agency*. s.l.:s.n.
- Iriarte-Cornejo, C., Arancibia-bulnes, C. A., Salgado-transito, I. & Weissman, J., 2014. ScienceDirect Compensation of heliostat drift by seasonal sampling. *Solar Energy*, Volume 105, pp. 330-340.
- Khalsa, S.S.S., Ho, C.K. and Andraka, C.E. 2011. An Automated Method to Correct Heliostat Tracking Errors. In: *SolarPACES Conference. SolarPaces2011*, Granada, Spain.
- Kribus, A., Vishnevetsky, I., Yogev, A. & Rubinov, T., 2004. Closed loop control of heliostats, *Energy*, vol. 29, no. 5-6, pp. 905–913.
- Larmuth, J., Malan, K. & Gauché, P., 2014. Design and cost review of a two square metre heliostat prototypes. *Proceedings of SASEC 2014*.
- Malan, K. & Gauché, P., 2013. Model based open-loop correction of heliostat tracking errors. *Energy Procedia*, 49(0), pp. 2118-2124.
- Malan, K.J. (2014). A Heliostat Field Control System., no. March. Available at: <http://scholar.sun.ac.za/handle/10019.1/86674>. [2017, July 20].
- Malan, K. J. & Gauché, P., 2014. A LOCALLY DEVELOPED 40 m² HELIOSTAT ARRAY WIRELESS CONTROL SYSTEM. *Proceedings of SASEC*, pp. 1-7.
- Mavis, C. L., 1988. *10 MWe Solar Thermal Central Receiver Pilot Plant Heliostat and Beam Characterization System Evaluation, November 1981-December 1986*. SAND 87-8003, Sandia National Laboratories, Livermore, CA, May 1988.
- Quero, J. M., Aracil, C., Franquelo, L. G., Ricart, J., Ortega, P. R., Dominguez, M., Castañer, L. M, and Osuna, R., 2007. Tracking control system using an incident radiation angle microsensors. *IEEE Transactions on Industrial Electronics*, vol. 54 no 2, pp. 1207-1216.
- Roos, T., Zwane, N., Kruger, E., Perumal, S., Cathro, R. C., 2009. A 25m² Target-Aligned Heliostat with Closed-Loop Control, *Presented at ISES SWC2007, Beijing*.
- Schell, S., 2011. Design and evaluation of esolar's heliostat fields. *Solar Energy*. 85. 614-619.
- Stone, K. W. & Jones, S. A., 1999. *Analysis of Solar Two heliostat tracking error sources*. Tech. Rep. SAND99-0239C, Sandia National Laboratories, Albuquerque, NM, USA.
- Zavodny, M., Slack, M., Huibregtse, R. & Sonn, A., 2015. Tower-based CSP Artificial Light Calibration System. *Energy Procedia*, Volume 69, pp. 1488-1497.

Appendix A. Photos of calibrated sunspots

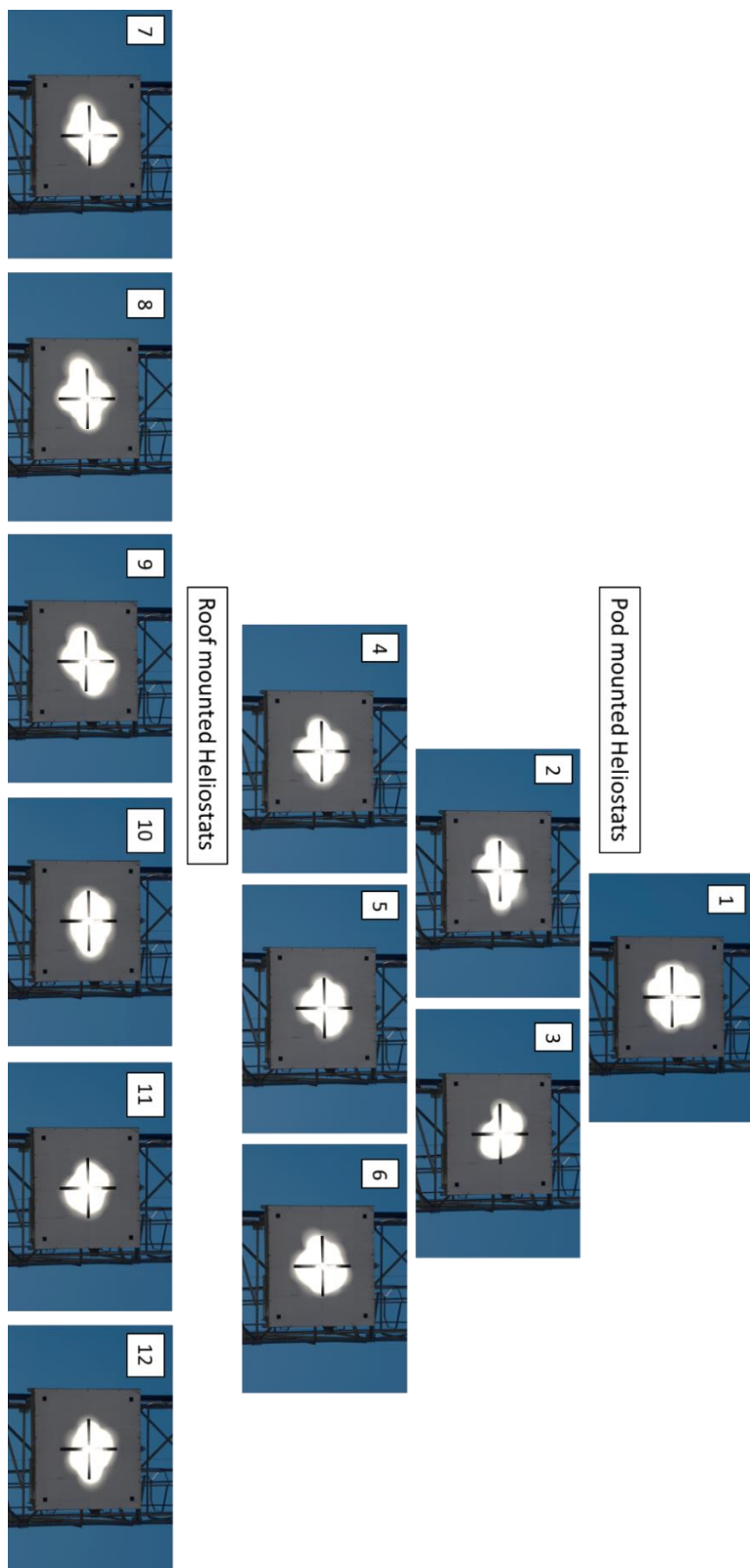


Figure A.1: Photos of all 12 calibrated heliostats reflecting onto the calibration target.

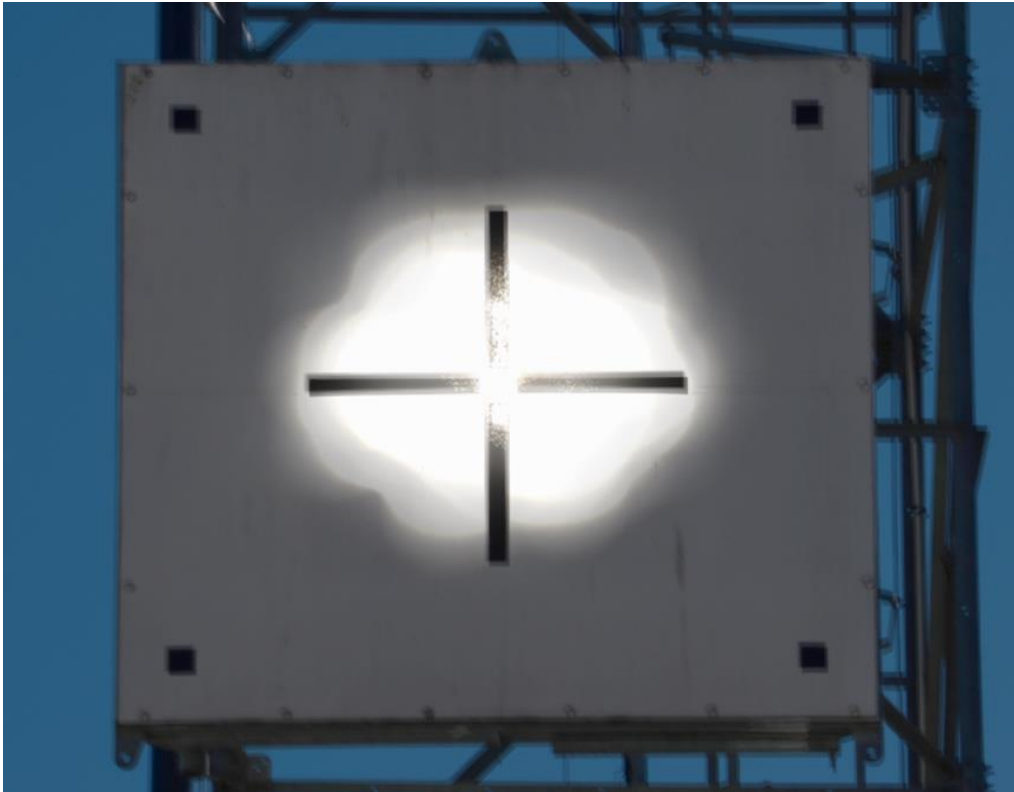


Figure A.2: All 12 individual photos superimposed

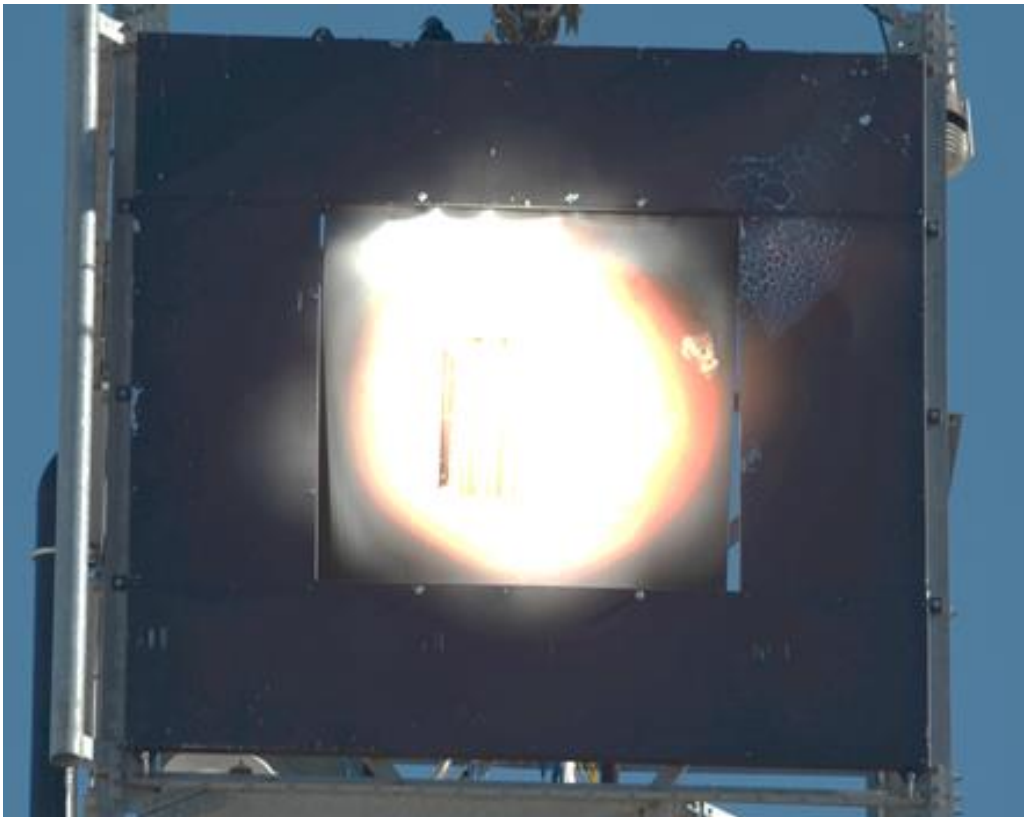


Figure A.3: All 12 heliostats reflecting onto the receiver